# Uncertainty of Porosity-Permeability Relationships from REV-scale Numerical Fluid Simulations

Ruben Zijlstra

February 24, 2022

## Abstract

Empirical porosity-permeability and grain size-permeability relationships have long been used and researched. However, they often under- or overestimate permeability because they simplify complex micro scale porous medium descriptions, such as tortuosity or pore size distribution, into nondescript parameters or constants. This paper aims to highlight the large range of possible permeability values that can be obtained from identical porosity and grain size distributions, but describe different pore scale porous media. To achieve this, numerical flow simulations were performed on irregular grained and circular grained porous media which contain identical grains and porosity but vary in spatial distribution of the grains within the domain. Subsequently, the domain was analyzed in terms of representative elementary volume, pore size distribution, grain size distribution, quantitative grain morphological parameters, porosity, and permeability. The results were compared to five well known empirical relationships: Hazen (1892), Slichter (1898), Beyer (1964), Kozeny-Carman (1953), and Barr (2001). Results showed a linear relationship between permeability on a logarithmic scale and porosity on an arithmetic scale with uncertainty increasing as porosity increased. Porous media containing equally sized circular grains as irregular grains in terms of sieve radius showed higher permeability values. Empirical relationships correctly captured the impact of porosity on permeability, but were unable to yield correct values, and even deviated by over a factor 10 for some porous media. This study emphasizes the need for more extensive research into pore scale processes influencing permeability and provides ideas for future research.

# Contents

# 1 Introduction

Determination of the capacity and ability of a soil to transmit fluids has been a long-standing problem of great practical relevance [*Koponen et al.*, 1997]. This parameter, called the permeability ($k$), is extensively used in scientific fields and hydrological engineering for example in estimation of slope stability, water inflow into construction sites, $CO_2$ storage, movement of contaminants in the subsurface, and construction of hydraulic barriers in contaminated sites [*Nishiyama and Yokoyama*, 2017; *Živković et al.*, 2021]. The precision in which $k$ needs to be determined varies, but may sometimes be required to be very accurate if not exact.

The concept of permeability was first introduced by Darcy through Darcy's law. It states that in laminar flow regimes, described by a low Reynolds number, fluid flow through the porous medium, a solid material which is partially filled by interconnected voids (pores) [*Dagan et al.*, 2008], under an applied pressure gradient can be described by Darcy's law as:

$$q = -\frac{k}{\mu}\nabla P \tag{1}$$

where q is the fluid flux in $[m/s]$, k is the permeability in $[m^2]$, $\mu$ is the dynamic viscosity of the fluid in $[Pa \cdot s]$, and $\nabla P$ is the applied pressure gradient in $[Pa]$ [*Matyka et al.*, 2008]. Permeability is an intrinsic property of the porous medium and depends on properties such as the porosity ($\theta$), which is a measure of the void space between grains, pore sizes, tortuosity ($\tau$), which is the deviation of the flow from a straight path, and surface roughness of the grains [*Živković et al.*, 2021]. Therefore, it does not depend on properties of the fluid. Darcy's law was determined empirically in the $19^{th}$ century and since then many researchers have tried to find a value for $k$ and its relationship to soil parameters such as $\theta$, grain sizes and shapes, and composition of the medium.

Various methods can be used to obtain $k$, each having different costs, advantages and disadvantages. The value can be determined experimentally in the field using the pumping-well method or at the column scale using for example the falling head method. It can also be obtained from statistical or capillary models or through empirical relationships [*Wang and Tong*, 2014; *Živković et al.*, 2021]. Since field and laboratory studies are quite tedious and time consuming, often porosity-permeability or grain size-permeability relationships are used.

Empirical relationships can be written as a general formula as:

$$k = cf(\theta)d^2 \tag{2}$$

where $k$ is the intrinsic permeability $[m^2]$, $f(\theta)$ a function of the porosity, $c$ is a dimensionless parameter which usually describes the porous medium in terms of $\tau$, connectivity of pores, or shapes, and $d$ is the particle diameter [*Shepherd*, 1989; *Nishiyama and Yokoyama*, 2017].

*Hazen* [1892] was the first to define a relationship between effective grain size and permeability as:

$$k \sim d_{10}^2 \tag{3}$$

where $d_{10}$ is the effective grain diameter indicating where 10% of the grains are finer [*Cabalar and Akbulut*, 2016].

Further research by Kozeny and later modified by Carman yielded perhaps the most well known empirical relationship: the Kozeny-Carman equation. It was derived from the Navier-Stokes equation using the capillary tubes model. The Kozeny-Carman equation predicts that a relationship exists defined as:

$$k \sim \frac{\theta^3}{(1-\theta)^2} \tag{4}$$

where $k$ is the permeability $(m^2)$, and $\theta$ the porosity [*Hommel et al.*, 2018; *Chapuis and Aubertin*, 2011].

The influences of shape characteristics on permeability were first studied by *Terzaghi* [1925] by testing flat-grained particles. It was later noted by *Gilboy* [1928] that any analysis which neglected the effect of grain shape would yield false results [*Cabalar and Akbulut*, 2016].

The problem with these and other semi-empirical relations is that none yield accurate and exact results. Many researchers have tried to formulate modified versions or calibration to, for example, the Kozeny-Carman equation

but these are often designed for a specific case study [*Nomura et al.*, 2018; *Krauss and Mays*, 2014; *Ruan and Fu*, 2021; *Lala*, 2018]. To use these relationships at the field scale, many samples are needed and heterogeneity of the site is often underrepresented. Experimental analysis done by *Rosas et al.* [2014] into hydraulic conductivity of different sediment samples compared to porosity-permeability relationships showed that no relation could obtain accurate values. After calibration results were more accurate, but some still deviated significantly from experimental values.

These relationships assume that any system described by a median grain size diameter and a porosity value are exactly the same, while in reality this is often not the case. Extensive and detailed knowledge of the pore sizes and spatial arrangement of the pore channels would be required to yield accurate permeability values [*Costa*, 2006]. Moreover, they often lack descriptions of the domain such as grain morphology [*Hommel et al.*, 2018]. No simple equation can be formulated that describes the complex system known as fluid flow through a porous medium. While the range of error when using these empirical relationships is quite significant, they are still being used to predict permeability.

Here, representative elementary volume (REV)-scale domains that are described by the same grain size distribution and porosity are generated where subsequent numerical fluid simulations allow the calculation of permeability. Different grain shapes and sizes are used to show that permeability cannot be accurately estimated using two simple soil parameters. Irregular shaped grains are analyzed in terms of sieve radius and morphological parameters such as sphericity and roundness. Thereafter, REV-scale domains using the same grain radii but with spherical shapes are generated to determine a link between porosity, grain and pore size distributions, and grain morphological parameters to better understand the impact of the porous medium on the permeability.

The aim of this research is to develop an easily adaptable REV scale numerical flow model which can be used to study the relationship between porosity, grain and pore size distribution, grain morphology and permeability. The model must be able to generate round and irregularly shaped grains or use grain shapes taken from a x-ray tomography sample and generate a domain in which numerical flow simulations can be performed. The ability to calculate empirical relationships, such as the Kozeny-Carman equation, and comparison to numerical results is also intended.

To show the applicability of the model, this paper set out to answer several research questions:

- What is the impact of spatial arrangement of identical grains on the permeability?
- What is the impact of grain size distribution and porosity on the permeability as calculated from numerical simulations and empirical relationships?
- What is the impact of grain morphology such as sphericity, and roughness on permeability?
- How is the uncertainty of permeability at the REV-scale related to properties of the porous medium?

## 2 Methods & Theory

Here, a pore scale flow model was used to simulate flow in different realizations of a porous medium with the same grain sizes and shapes but different spatial arrangement. Through this Monte Carlo method we identify the permeability uncertainty that comes from spatial distribution of identical grains. Morphological descriptions of grains were used to find a correlation between average grain shape and permeability between irregular and round grains of equal grain size distribution.

Bram van der Hoek created a python-adapted workflow of a pore-scale grain generator built by Enno de Vries. To achieve our goal, the workflow was updated and adapted. In its original state, the model was able to generate realizations of porous media within a porosity range containing circular grains, the radius of which is taken from a grain size distribution. Furthermore, it was able to place those grains inside a domain, and perform computational fluid dynamics simulations using OpenFOAM and extract and post-process results to obtain values for local velocities, pressure and porosity. These values were used to solve the Darcy equation for 1D fluid flow, giving the permeability value.

The model was updated from its original state by adding a method of performing Monte Carlo simulations. This allowed a single porosity to be taken and grain placement to be varied by generating a uniform distribution of randomized x and y values. Irregular shaped grains were generated using a newly implemented function, but could also be created from a list of pre-generated shapes. Permeability of the domain was also calculated using five empirical porosity-permeability relationships to compare to simulation results. To obtain values for

these relationships, grains radius was analyzed using two methods. To describe the porous media in a more quantitative way, morphological grain parameters and pore size distributions were calculated.

## 2.1 Domain Generation

To generate the domain, the following procedure was used (Fig. 1). A random radius was taken from the input grain size distribution curve, which could be given as either a truncated log-normal distribution or as a grain sieve analysis data set where sieve holes and percent passing are specified. This radius was used to generate a shape, of which the area was calculated. The area can be calcualted in two ways: through use of the Shapely module [*Gillies et al.*, 2007] or through the mathematical formulation of the area of a polygon. For the Shapely method, the points of the polygon are assigned to a polygon object of which the area can be calculated. The mathematical formula for calculating the area of a polygon is defined as:

$$A_g = \left| \frac{(x_1 y_2 - y_1 x_2) + (x_2 y_3 - y_2 x_3) ... + (x_n y_{n+1} - y_n x_{n+1})}{2} \right| \tag{5}$$

where $A_g$ is the area of the current grain, $x_n$ is the x coordinate of vertex $n$, and $y_n$ is the y coordinate of the $n^{th}$ vertex. Though Shapely is less trivial in understanding, computational time is longer than the mathematical expression given above.

With the calculated area and the specified domain boundaries, the porosity can be calculated as:

$$\theta = 1 - \frac{\sum A_g}{A_{tot}} \tag{6}$$

where $\sum A_g$ is the sum of the area of the grains as calculated from Eq. (5) or shapely, and $A_{tot}$ is the total area of the domain obtained from:

$$A_{tot} = (x_{max} - x_{min})(y_{max} - y_{min}) \tag{7}$$

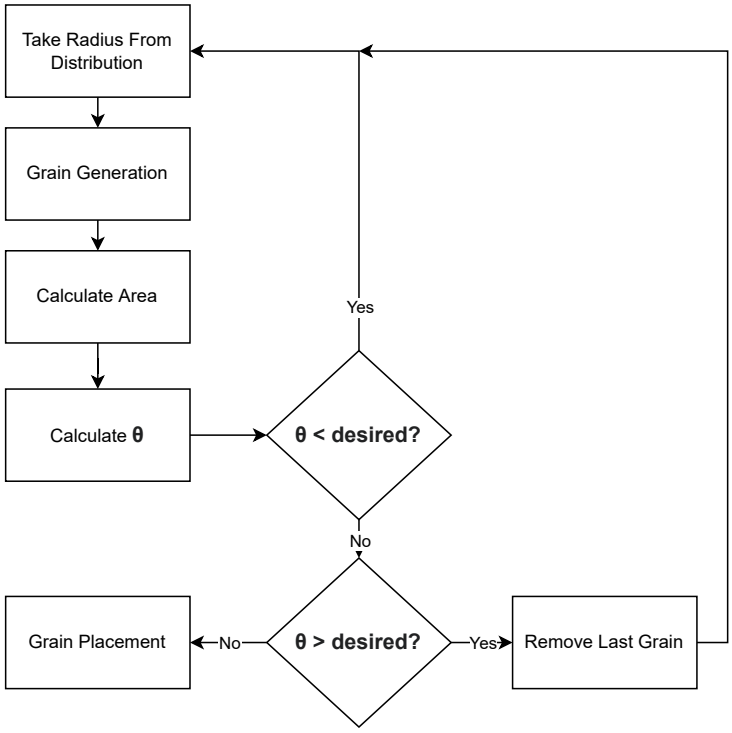


**Figure 1:** *Workflow of the grain generation and subsequent placement within the domain.*

where $x_{max}$, $x_{min}$, $y_{max}$, and $y_{min}$ are the minimum and maximum coordinates of the domain in $[L]$. More random grain radii will be drawn from the distribution and used to calculate $\theta$ until the desired $\theta$ is reached. If required, a seed can be set to make grain generation reproducible. The code will then continue with placing the grains within the domain.

A specified number of points was used to generate random x and y values from a uniform distribution with the lower and upper boundary being the length of the domain. Placing of grains was done by translating the vertices of each grain by this random x and y value. Later, when generating a cell grid of the domain for numerical flow simulations, a minimum of two cells for the smallest possible pore throat is necessary. If this is not done, unintentional dead end pores are created which affect permeability calculated from flow simulation results. The cell size is defined by the minimum distance which is specified at the start of the domain generation. To achieve this, the grains were enlarged by the minimum distance before placement. After placement, grains were reduced in size by this same minimum distance. When placing a grain, three checks had to be done in order to make sure the grain was placed correctly:

1. Is there overlap with inlet or outlet
2. Is there overlap with top or bottom of domain
3. Is there overlap with any previously placed grains

Checking the overlap with either: inlet, outlet, top or bottom was done with use of the Shapely package. Shapely contains a function where overlap with a line and a polygon can be calculated, if this is the case it returns either true or false. When the grain overlaps with the inlet or outlet, the original grain was translated to a different location and checked again.

Grain overlap with the top or bottom of the domain is a unique circumstance. If this occured, another grain with the same size and shape was placed at the opposite side of the domain (Fig. 2). This was done with two reasons in mind: the first was to minimise wall effects that occur during flow simulations by introducing this periodicity, the second to ease calculation of $\theta$. This means that a grain that was partially in the domain, will be fully in the domain when placed at the other boundary. Therefore, the total area of that shape within the domain is constant.

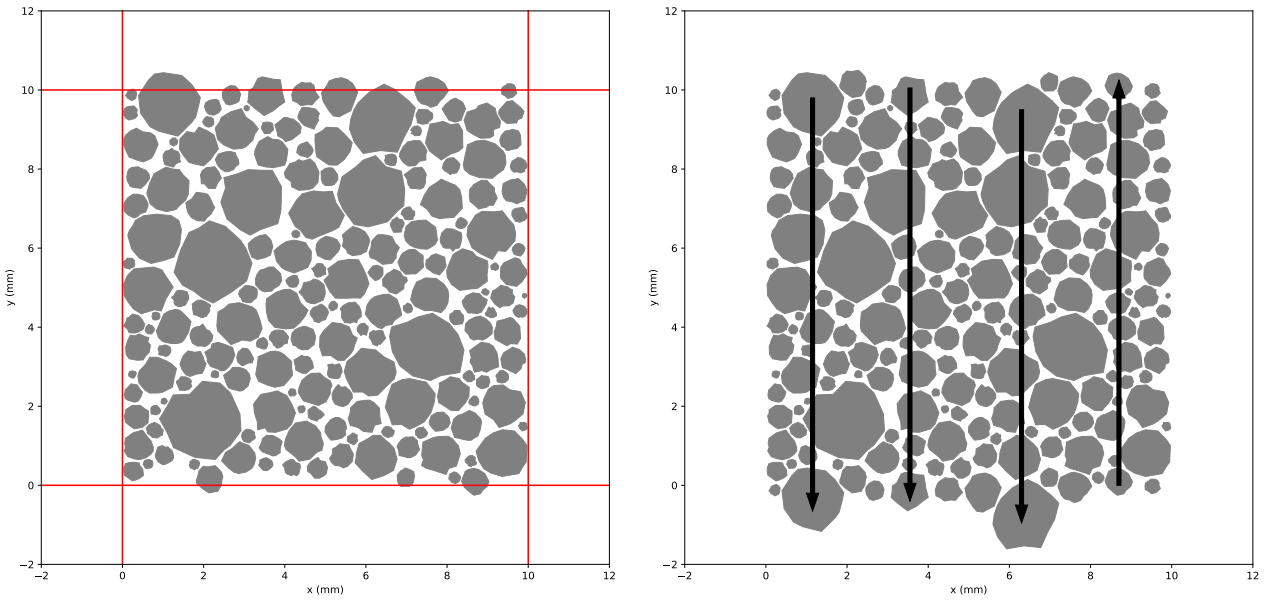


**Figure 2:** *Grain periodic boundary condition where grains overlapping the domain at the top or bottom, indicated by the red box, are placed at the other side of the domain as indicated by the black arrows.*

Overlap with another grain was checked in an almost identical way. However, instead of checking overlap with a line and a polygon, overlap between two polygons was checked. If the grain happened to be a top or bottom boundary grain, the duplicated grain at the other side of the domain was also checked for overlap against any other grains. If overlap occurred, the original grain was translated to a new location and the three checks were done again until no overlap occurred. The grain was then stored and the code moves on to find a suitable location for the next grain.

Grains were placed from large to small, to ensure that every grain could be placed. However, sometimes a grain failed to be placed within the domain due to grains being similar or too large in size. That grain was then skipped and all subsequent grains were tried. A new $\theta$ was calculated and saved to compensate for this failure.

## 2.2 Generation of Irregular Grain Shapes

The old code was able to take a radius from a truncated log-normal distribution or from sieve analysis data. A random radius was taken from the distribution and could be used in the generation of a circular grain without defining the exact location of the boundary of the grain. For example, when checking for overlap, only a comparison of the center point of two grains and their respective radii was needed. When checking the overlap of two random shapes, the location of the edges are also needed. Therefore, irregular shaped grains were generated as polygons with a set number of vertices (Fig. 3). Vertices are coordinate points each with an x and y value. Vertices were generated based on a radius, and an angle between points which was converted from Polar to Cartesian coordinates. When the angle between points and radii are kept constant, a circular grain is created. Therefore, the angle and radii are varied to obtain more irregular shaped grains. The number of vertices was given as input at the start of the grain shape generation.

The angle between each vertex is defined as:

$$\Theta_n \sim U(\frac{2\pi}{N} - I, \frac{2\pi}{N} + I) \tag{8}$$

where $\Theta_n$ is the angle between vertex point $n$ and $n+1$, $N$ is the total number of desired vertex points, $U$ is a uniform distribution, and $I$ the irregularity parameter with a value between zero and one. The angles are normalized as:

$$\Theta_n = \Theta_n \frac{2\pi}{\sum \Theta_n} \tag{9}$$

This is done to ensure that the total internal angle is equal to $2\pi$, and therefore the first and last point are the same. To generate a random radius, a Gaussian distribution is defined as:

$$r_n \sim \mathcal{N}(\mu, \sigma^2) \sim \mathcal{N}(r_i, r_v^2) \tag{10}$$

where $r_n$ is the random radius of the $n^{th}$ vertex, $r_i$ is a random radius as taken from the input grain size distribution, and $r_v$ is the radius variance parameter with a value between zero and one. The value of $r_n$ was truncated between zero and $2r_i$ to prevent creation of extremely spiked shapes.

To generate more randomness in the shape, the initial angle used to generate the shape was set to a random value between 0 and $2\pi$, subsequently the previously generated $\Theta_n$ was added to this for each calculation of x and y:

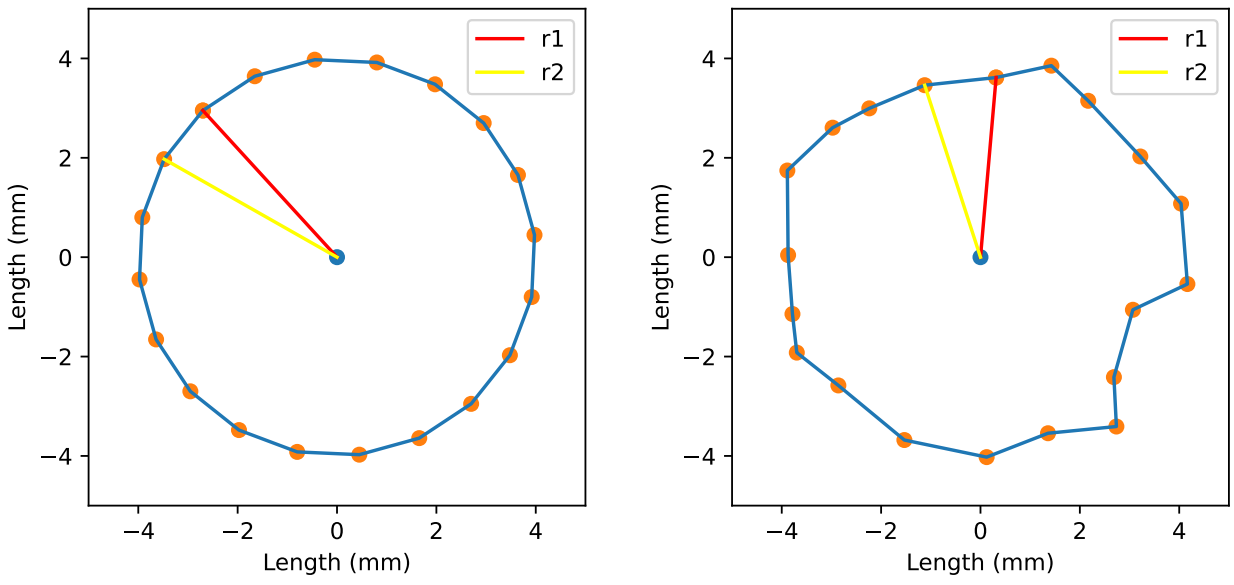


**(a)** **(b)**

**Figure 3:** *Generation method of a circular and irregular shaped polygon with input radius ($r_i$) of 4mm. (a): The shape of grain without altering angle between subsequent vertex points and no alteration of the input radius. (b): Random grain shape generated using radius variance ($r_v$) of 0.1, 20 vertex points and variance between vertex angles ($I$) of 0.6.*

$$\phi_0 = z \tag{11}$$

$$\phi_n = \phi_{n-1} + \Theta_n \tag{12}$$

where z is the starting angle with a random value taken from a uniform distribution between 0 and $2\pi$, $\phi$ the total current angle and $\Theta$ the difference in angle (Eq. (9)).

The angle and radius are converted from Polar to Cartesian coordinates as:

$$x = x_c + r_n * \cos(\phi_n) \tag{13}$$

$$y = y_c + r_n * \sin(\phi_n) \tag{14}$$

where $x_c$, and $y_c$ are the center point coordinates, initially: (0,0), $r_n$ is the radius taken from a Gaussian distribution, and $\phi_n$ is the current total angle.

## 2.3 Flow Simulations

Simulation of fluid flow through the domain was done with use of OpenFoam. OpenFoam is a toolbox that numerically solves flow and transport equations typically found in computational fluid dynamics making use of the finite volume method [*Muhammad*, 2021]. SimpleFoam is an algorithm within OpenFoam that solves steady-state, incompressible, turbulent flow by solving equations for continuity:

$$\nabla \cdot u = 0 \tag{15}$$

and momentum:

$$\nabla \cdot (u \otimes u) - \nabla \cdot R = \nabla p + S_u \tag{16}$$

where $u$ is the velocity, $p$ the kinematic pressure, $R$ the Stress tensor, $\otimes$ the outer product, and $S_u$ the momentum source. These equations were solved numerically by taking the solution of the previous time-step and using this as input for the calculation of the state variables in the next time-step. The inlet and outlet of the domain were set to a fixed pressure value of $1.0 * 10^3$ and 0 Pa, respectively.

Turbulent flow settings can be disabled if laminar flow can be assumed, which is the case for Reynolds number smaller than 160 [*Dybbs and Edwards*, 1984]. Reynolds number (Re) is calculated as:

$$Re = \frac{uL_c}{v} \tag{17}$$

where $u$ is the flow velocity in $[m/s]$, $L_c$ is the characteristic length in $[m]$, and $v$ is the kinematic viscosity in $[m^2/s]$. The Reynolds number should represent the flow condition, for example, in a pipe the characteristic length is taken as the diameter of that pipe. Here the minimum distance of the pore throat, 0.025mm or $2.5 * 10^{-5}m$ was taken as $L_c$. For the flow velocity, the average value of preliminary tests using the previous model were used. Other values used to calculate Reynolds number are: $10^{-6}m^2/s$, and $5.38 * 10^{-5}m/s$ for kinematic viscosity and flow velocity, respectively. This resulted in a Re of 0.00134 which is below 160 and therefore laminar flow was assumed.

After flow simulations converged, the permeability can be calculated from Darcy's law:

$$k = -\theta v u_{mean} \rho \frac{dx}{dp} \tag{18}$$

where $\theta$ is the porosity, $v$ is the kinematic viscosity in $[m^2]$, $\rho$ the density of the fluid in $[kg/m^3]$, $u_{mean}$ is the mean flow velocity in the x-direction in $[m/s]$ and $\frac{dx}{dp}$ is the inverse pressure gradient in the x-direction. It should be noted that openFoam is configured to use kinematic pressure which is defined as:

$$p = \frac{P_s}{\rho} \tag{19}$$

where $P_s$ is the static pressure in $[Pa]$ and $\rho$ the density of the fluid in $[kg/m^3]$. Therefore, to use normal static pressure in Eq. (18), the pressure was multiplied by the density of the fluid. But since the inverse pressure gradient is required, a division by density is required, thereby the permeability formula becomes:

$$k = -\theta v u_{mean} \frac{dx}{dP_s} \tag{20}$$

OpenFoam simulation results were written to a VTK file, which was used as input for obtaining the required parameters. Porosity is re-calculated as:

$$\theta = \frac{A_{cells}}{A_{tot}} \tag{21}$$

where $A_{cells}$ is the total cell volume obtained from the grid created by BlockMesh and SnappyHexMesh, and $A_{tot}$ is the total size of the domain obtained from Eq. (7).

## 2.4 Porosity-Permeability Relationships

Various methods of calculating permeability from the grain size distribution and porosity exist and the most notable ones are summarized in *Devlin* [2015]. These relationships can be described in a general equation as:

$$k = cf(\theta){d_e}^2 \tag{22}$$

where $c$ is a case-specific constant which is often described as a shape parameter, $f(\theta)$ is a function of porosity, and $d_e$ is the effective grain size as taken from the grain size distribution. Here the porosity is taken as the re-calculated porosity from the VTK file and the effective grain size is taken from the grain size distribution curve calculated in the next section.

Work done by *Lin* [2021], which compared laboratory and empirical permeability values for various porosity and grain size distributions yielded five relationships that showed good correlation: *Hazen* [1892], *Slichter et al.* [1898], *Beyer* [1964], *Kozeny* [1953], and *Barr* [2001]. These relationships (Table. 1) were used for comparative analysis in this work.

| **Name** | **c** | $\boldsymbol{f(\theta)}$ | $\boldsymbol{d_e}$ | **Conditions** |
|---|---|---|---|---|
| Hazen (1892) | $6.4 \times 10^{-4}$ | $1 + 10(\theta - 0.26)$ | $d_{10}$ | $0.1 \text{ mm} < d_{10} < 3.0 \text{ mm}$<br>$U < 5$ |
| Slicher (1898) | $1 \times 10^{-2}$ | $\theta^{3.287}$ | $d_{10}$ | $0.1 \text{ mm} < d_{10} < 5.0 \text{ mm}$ |
| Beyer (1964) | $5.2 \times 10^{-4} \log \frac{500}{U}$ | 1 | $d_{10}$ | $0.06 \text{ mm} < d_{10} < 0.6 \text{ mm}$<br>$1 < U < 20$ |
| Kozeny-Carman (1953) | $8.3 \times 10^{-3}$ | $\frac{\theta^3}{(1-\theta)^2}$ | $d_{10}$ | Coarse sand |
| Barr (2001) | $\frac{1}{(36)5{C_s}^2}$<br>${C_s}^2 = 1$ for spherical grains,<br>${C_s}^2 = 1.35$ for angular grains | $\frac{\theta^3}{(1-\theta)^2}$ | $d_{10}$ | None |

**Table 1:** *Permeability-porosity relationships following Devlin [2015], specifying a case-specific constant c, function of porosity $f(\theta)$, and the effective grain size $d_e$ for permeability calculation using Eq. (22). $U$ is the uniformity defined as $\frac{d_{10}}{d_{60}}$.*

## 2.5 Post-Processing: Grain Analysis

### 2.5.1 Grain Size

The initial grain size distribution was used to generate irregular random shapes, which will after alteration no longer follow that distribution. For example when altering a circle with a diameter of 1 mm to an ellipse, that shape can no longer be described in terms of a radius of 1 mm. Therefore, a method is necessary to analyze the radii of the grains in a quantitative way. Two methods for analyzing the grain size distribution were implemented.

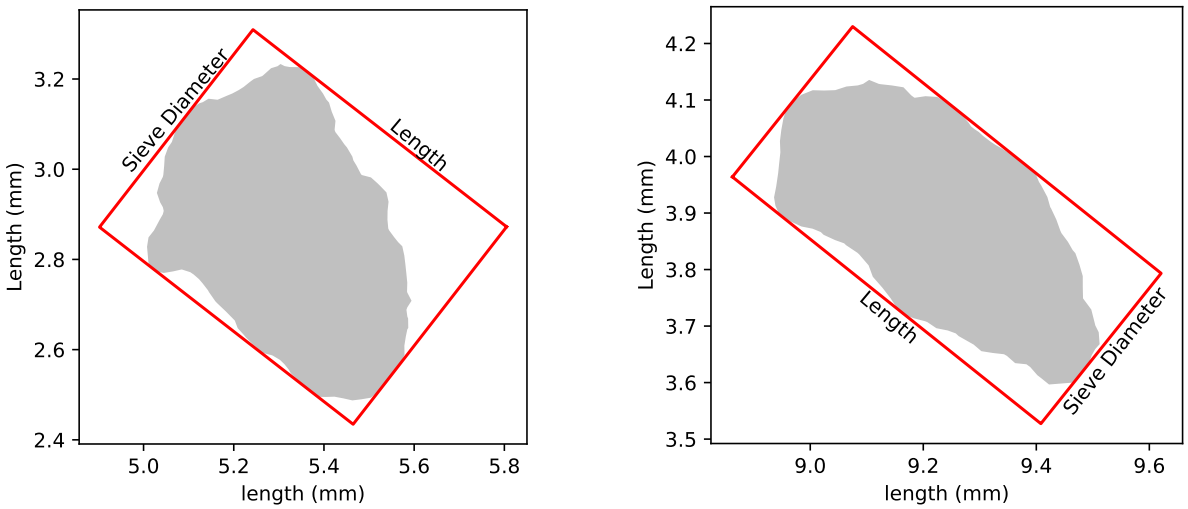


**(a)** **(b)**

**Figure 4:** *Determining the smallest width and length of a irregular shaped polygon using the minimum bounding box method. Grain size is taken as the smallest width as this would also pass through a screen size of similar size. (a): 0.555 mm, (b): 0.341 mm*

The first method calculates the equivalent radius, which is the radius of a circle with an equivalent area as that shape [*Lopez-Sanchez and Llana-Fúnez*, 2014]. The equivalent radius ($r_{eq}$) is calculated from:

$$r_{eq} = \sqrt{\frac{A}{\pi}} \tag{23}$$

where $A$ is the area of the polygon in $[m^2]$ and $r$ is the radius in $[m]$. The area ($A$) is calculated from either the Shapely module or from Eq. (5).

While this method can be very easily used in simulations, determining the area of particles in real life could prove nearly impossible for large scale or even small scale research. Therefore, we also implemented a second method which is more comparable to how a sediment sample is analysed in the lab.

The second method places a bounding box around the particle, from which the polygon width and length can be obtained (Fig. 4). It works by using a Shapely function which finds the smallest area possible that encompasses all given points, in this case: the vertices. This gave a minimum width that was needed to pass through a sieve hole when filtering sand particles. *Blott and Pye* [2008] analyzed different methods of determining length and width for particles and found that using the smallest bounding box possible yielded the most accurate description of the size of a gravel particle.

From the radii, the grain size distribution curve (Fig. 5) was constructed. For this, the cumulative frequency and the desired sieve holes were needed. The frequency was calculated by comparing the current radius and checking if its smaller than a certain sieve hole diameter. The relative frequency of each bin is then calculated from:

$$f_i = \frac{f}{n} \tag{24}$$

where $f$ is the absolute frequency, while $n$ is the sum of all frequencies. The cumulative frequency for each data class was then obtained by adding the relative frequency of the previous data range to the current.

### 2.5.2 Grain Shape

While it has been shown that particle size is important when it comes to calculating the permeability of a system, the shape is often disregarded. Grain morphology is of interest in geology since it tells us something about transportation and depositional enviroment [*Tunwal et al.*, 2018]. *Göktepe and Sezer* [2010] found that shape has a strong effect on the permeability. However, they were limited by field data availability which can be overcome by the use of the model presented in this work.

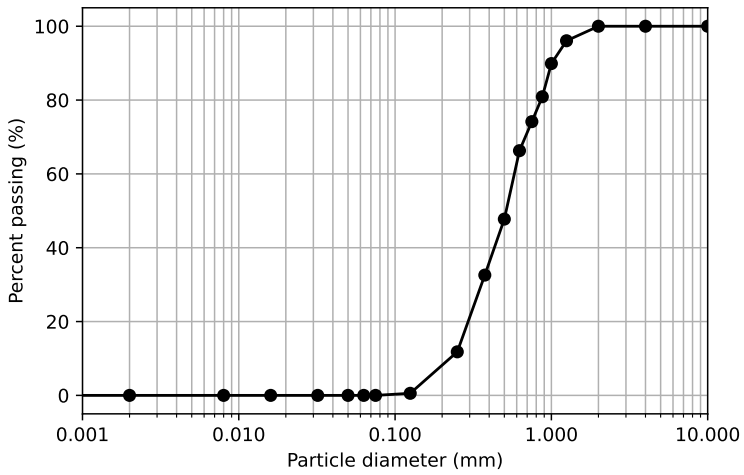


**Figure 5:** *Typical grain size distribution curve as obtained from a sieve analysis of a sample*

A single grain shape parameter is not always able to characterize the uniqueness of a shape. For example, a value for sphericity may describe either a rectangle or a random shape which by chance has the same ratio between circumscribed and inscribed circle radius. To overcome this problem, multiple parameters were used to describe the generated shapes. In this study, sphericity, circularity, solidity, and roundness were implemented. The relative importance of each of these in terms of grain description is still unclear [*Blott and Pye*, 2008; *Tunwal et al.*, 2018], therefore while choosing the parameters the ease of implementation was weighed more heavily. All parameters are dimensionless to keep them seperate from the grain size determination.

Angularity may also pose an interesting parameter as it is used as another parameter describing roundness in literature. However its implementation proved difficult based on current research [*Tunwal et al.*, 2018]. It has also been found that the length and width obtained from the bounding box method as described in section 2.5.1 can be used to determine parameters such as compactness, elongation and rectangularity but this is a matter for future research.

### 2.5.3 Grain Shape: Sphericity

The exact definition of sphericity is unclear, various articles use this shape description interchangeably with that of roundness or circularity. Here the definition as given by [*Riley*, 1941] is taken, which states that the sphericity is a measure of the similarity of a shape to a perfect circle [*Tunwal et al.*, 2018]. Sphericity is calculated as:

$$\phi_0 = \sqrt{\frac{i}{D_c}} \tag{25}$$

where $i$ denotes the diameter of the inscribed circle, and $D_c$ the diameter of the circumscribed circle (Fig. 6).

To find the largest inscribed circle, an algorithm called "the pole of inaccessibility" or PIA was implemented. This is the point that lies within a polygon that is furthest away from the outlines of that polygon [*Garcia-Castellanos and Lombardo*, 2007]. Normally this algorithm is applied to find the point within a country that is furthest away from its borders. It was done using the polylabel function that is obtained from the Shapely library. The radius of the inscribed circle is then calculated as the smallest distance from the PIA to the nearest edge of the polygon.

To find the smallest circumscribed circle, a readily available technique from computational geometry was used. This method is called randomized incremental construction, where points are added randomly one by one and checked whether they fall within the initial circle estimate. For the exact working of this algorithm the reader is referred to *Welzl* [1991].

### 2.5.4 Grain Shape: Circularity

Just as sphericity, circularity is a measure of a particles resemblance to a circle. However, circularity takes into consideration the smoothness of the perimeter. Therefore, it described both the roughness as well as the

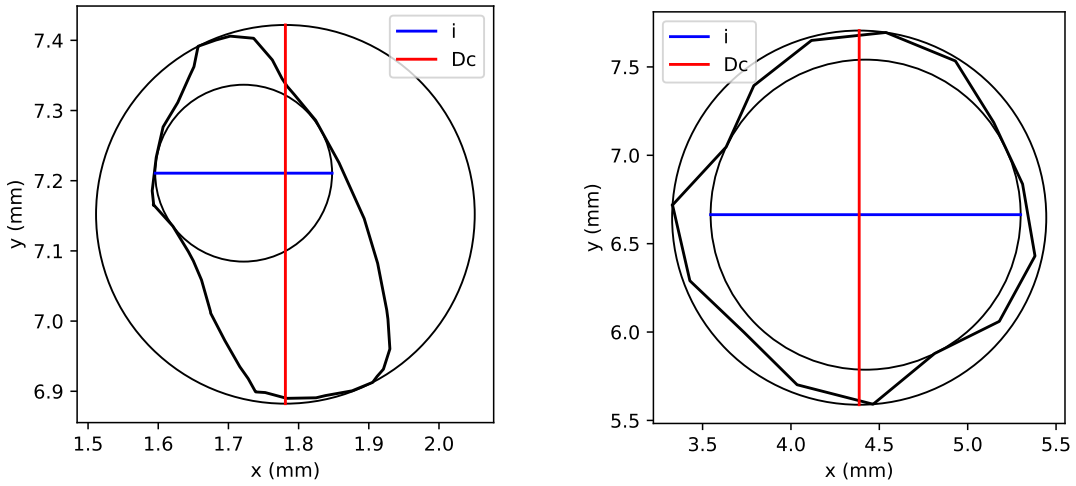


**(a)** **(b)**

**Figure 6:** *Random particle taken from pre-generated shape list (a), and a randomly generated polygon (b). Plotted with the shapes are the inscribed and circumscribed circle as well as their respective diameters. Here i, the inscribed circle diameter, is presented as the blue line and $D_c$, the circumscribed circle diameter, is given as the red line. The sphericity values are calculated from Eq. (25) as 0.683 (a) and 0.910 (b).*

morphology of the particle [*Olson*, 2011]. Circularity is effective in describing the roundness of particles, giving lower values for particles belonging to classes of higher roundness [*Dellino and La Volpe*, 1996].

Circularity ($C$) is calculated following *Roussillon et al.* [2009] as:

$$C = \frac{P_g}{2\sqrt{A\pi}} \tag{26}$$

where $P_g$ is the perimeter of the grain in [L], and $A$ is the area of the grain in $[L^2]$. The area is calculated from Eq. (5), and the perimeter is calculated as the length function from the Shapely library.

A perfect circle will have a circularity value of one, while values higher than one indicate less circular shapes. Values around 1.35 usually indicate slightly elongated grains. In literature, one may find the above equation in different forms but also the inverse is often used due to preference of values below zero indicating less rounded shapes.

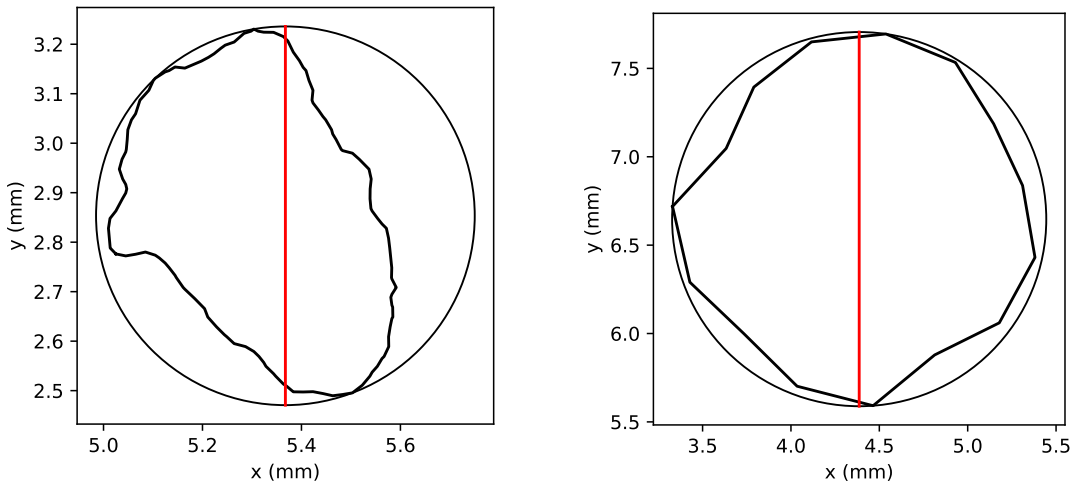


**(a)** **(b)**

**Figure 7:** *Random particle taken from pre-generated shape list (a) and a randomly generated polygon (b). Plotted with the shapes are the circumscribed circle as well as a red line representing its radius. The roundness values are calculated from Eq. (27) as 0.880 (a) and 0.949 (b).*

### 2.5.5 Grain Shape: Roundness

Roundness (Fig. 7) describes the curvature of a particle's corners. Originally, the roundness of a particle was formulated by *Wadell* [1932] and was defined as the ratio between the radius of circles fitted in the corners of the grain divided by the radius of the largest inscribed circle. However it has been found that the original method is quite difficult to apply [*Hayakawa and Oguchi*, 2005]. Therefore, an alternative calculation for roundness ($R$) as proposed by *Roussillon et al.* [2009], is used:

$$R = \frac{P_g}{D_c} \tag{27}$$

where $P_g$ is the perimeter of the grain, and $D_c$ is the perimeter of the smallest enclosing circle or circumscribed circle. This will yield values between 0 and 1, where 1 indicates a perfect circle and lower values indicate large particle curvature. When combining roundness formulated above with a compaction factor, which is a ratio between the length and width of the particle, the perimeter of the best fitted ellipse can be used. However, since here the compaction factor is not calculated, the perimeter of a circle is used instead.

## 2.6 Grain Shape: Solidity

Solidity is a measure of the overall concavity of a particle [*Olson*, 2011]. Solidity (S) is defined as:

$$S = \frac{A}{A_{eq}} \tag{28}$$

where $A$ is the area of the grain, and $A_{eq}$ is the area of the perimeter-equivalent circle [*Heilbronner and Barrett*, 2013]. This grain shape factor can also be written as:

$$S = \frac{4\pi A}{P_g^2} \tag{29}$$

where $P_g$ is the perimeter of the grain. Notably, this is the same as the cubed value of the inverse of circularity. Solidity has values ranging from 0 to 1. Rough particle edges are characterized by a low solidity, while smooth particle edges are characterized by a high solidity [*Mgangira et al.*, 2013].

## 2.7 Ensemble Settings

Two methods of defining the grain size distribution are available: using a truncated log-normal distribution or grain sieve analysis data. In a log-normal distribution, the natural logarithm of the data is normally distributed. The truncated log-normal parameters that have to be defined are $r_{min}$, which defines the lower truncation boundary of the distribution, $r_{max}$, which defines the upper truncation boundary of the distribution, $r_{mean}$, which defines the first moment of the non-truncated log-normal distribution, and $r_{std}$, which defines the second moment of the non-truncated log-normal distribution. The first and second moment of the log-normal distribution are converted into the first and second moment of the truncated log-normal distribution, and subsequently into the first and second moment of the truncated normal distribution. Input field data is defined as the cumulative frequency and associated grain radii in $mm$ obtained from sieve analysis.

Three different types of grain size distributions were generated (Table. 2): "homogeneous", "heterogeneous" (Fig. 8) and "pre-generated" with grain sizes determined by post-simulation analysis. While the Homogeneous distribution has a wider range of grain sizes as compared to the heterogeneous, the larger grains of the homogeneous grain size distribution will dominate within the domain. Therefore, the porous medium will appear to be homogeneous and thus be named as such. Examples of realizations of these different domain types can be found in the Appendix (Fig. A.1:A.6). A list of grain vertices for different shapes was obtained from 2D transformed x-ray tomography data. These were used in generating the pre-generated domain.

Monte Carlo simulations were performed on the placement of the grains to analyze the impact of grain positioning. A porosity within the specified range is taken, and a grain size distribution and associated irregular grains are generated and placed at random positions within a domain of 10 by 10 mm. Grain size and shapes are kept constant, but different realizations of the placement are created. OpenFoam then solves flow equations and permeability is calculated. Further output of the ensemble includes the actual $\theta$ value of the realization, grain vertex points as well as grains analyzed in terms of mono circle radius and radius determined with the bounding box method as described in section 2.5.1.

| Name | $r_{min}$ | $r_{max}$ | $r_{mean}$ | $r_{std}$ | I | $r_v$ | N | $\theta$ range |
|---|---|---|---|---|---|---|---|---|
| Homogeneous | 0.01 | 1.0 | 0.35 | 0.25 | 0.5 | 0.08 | 15 | 0.3 - 0.45 |
| | | | | | | | | 0.35 - 0.4 |
| | | | | | | | | 0.38 - 0.4 |
| | | | | | | | | 0.4 - 0.48 |
| Heterogeneous | 0.001 | 0.5 | 0.15 | 0.25 | 0.5 | 0.08 | 15 | 0.4 - 0.5 |
| Pre-generated | - | - | - | - | - | - | - | 0.45 - 0.65 |

**Table 2:** *Ensemble settings for the truncated log-normal distribution ($r_{min}$, $r_{max}$, $r_{mean}$, and $r_{std}$), irregular grains ($I$, $r_v$, and $N$), and porosity range ($\theta$). Pre-generated shapes do not follow a truncated log-normal distribution and therefore parameters are not specified for this ensemble. As homogeneous domains were the initial test of the model and cluster execution, different $\theta$ ranges were used.*

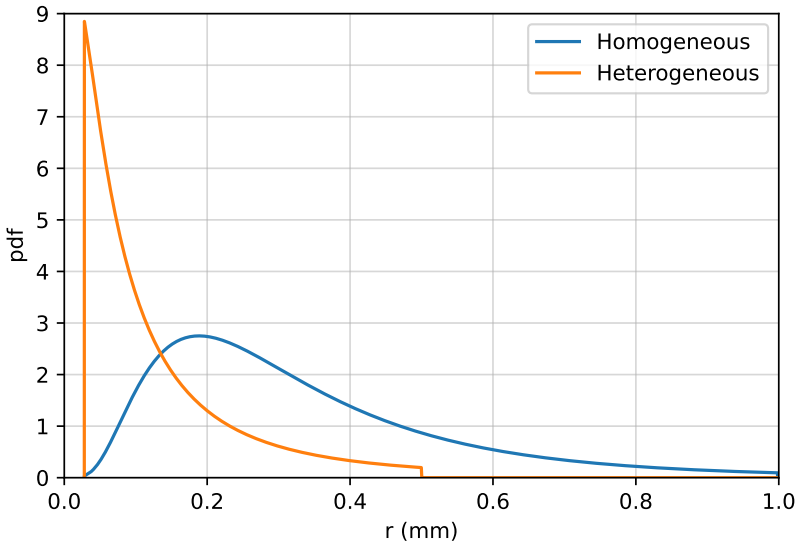


**Figure 8:** *Probability density function of the truncated log-normal distribution for the homogeneous and heterogeneous domains.*

The post-simulation analyzed grain radii were used as input for the circular grain simulations to analyze the impact of the irregularity of the grains. This means we used the same $\theta$ and grain size distribution, placed at different positions but now with circular grains instead of irregular ones. Since the number of grains in the "homogeneous" simulation is low, obtaining the same cumulative frequency curve for the radii is difficult. Therefore, the number of grains of the circular domain had to be increased. To do this, the maximum x value of the circular domain for these porous media was set to 20 mm instead of the regular 10 mm. This is not done for the "heterogeneous" or pre-generated domains as this contains smaller and, therefore, more grains.

Different methods for calculating the minimum distance between grains are employed during the placement of the circular and the irregular particles. When calculating the minimum distance between irregular particles, all of the particles are enlarged by the specified minimum distance at the start of the placement phase. Overlap between particles is checked and after placement has finished, grains are reduced in size by this minimum distance. This means that the actual minimum distance between the grains is double of the specified input. The minimum distance is only added to the grain placed at that moment during the sequential placement of circular grains. Meaning that the specified input minimum distance is the actual minimum distance. During the spherical simulations, the minimum distance was doubled from its value in the irregular grained simulations to correct for this. Here, the minimum distance for the irregular particles was set to 0.025 mm, for the circular particles this was set to 0.05 mm. Therefore, the minimum distance between grains for both domains was identical.

## 2.8 REV Tests

Physical modelling of flow in porous media is done on multiple length scales: pore- (microscopic), local (macroscopic), and field-scales [*Zhang et al.*, 2000]. Processes and equations on one scale might not describe the

situation or be applicable at the other. We need to determine whether our domain describes a representative elementary volume (REV) (Fig. 9). That is to say: do differences in permeability reflect changes within pore throats or do they represent changes of the domain as a whole. *Bear* [1972] first defined the REV as: "The smallest possible volume over which a measurement can be made that will yield a value representative of the whole volume". It is important to determine whether the domain can be described as REV as measurements made at REV scale are scale in-dependant and accurately represent a larger system [*Bear*, 1972]. The properties of the porous medium are related to the sample size and, therefore, determining the appropriate size is crucial to obtain a representative value of any soil property [*Borges et al.*, 2018].

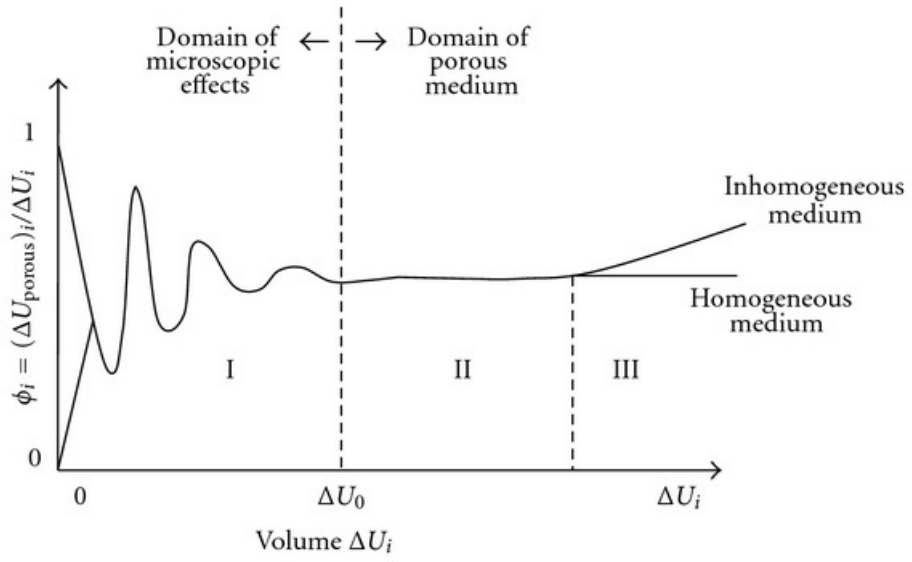


**Figure 9:** *Conceptual diagram of the representative elementary volume (REV) taken from Bear [1972]*

*Costanza-Robinson et al.* [2011] found that the average grain diameter is usually the best method of obtaining the REV magnitude, however, other properties of the porous medium such as $\theta$ or permeability may also be used. Here, the $\theta$ was used as this method is readily available in PoreSpy [*Gostick et al.*, 2019]. To determine if our domain could be described as REV scale, the $\theta$ of a small volume of the domain was calculated. The volume was increased and the $\theta$ was calculated again, repeating until the desired amount of measurements had been done. In this case the desired amount of measurements was 2000.

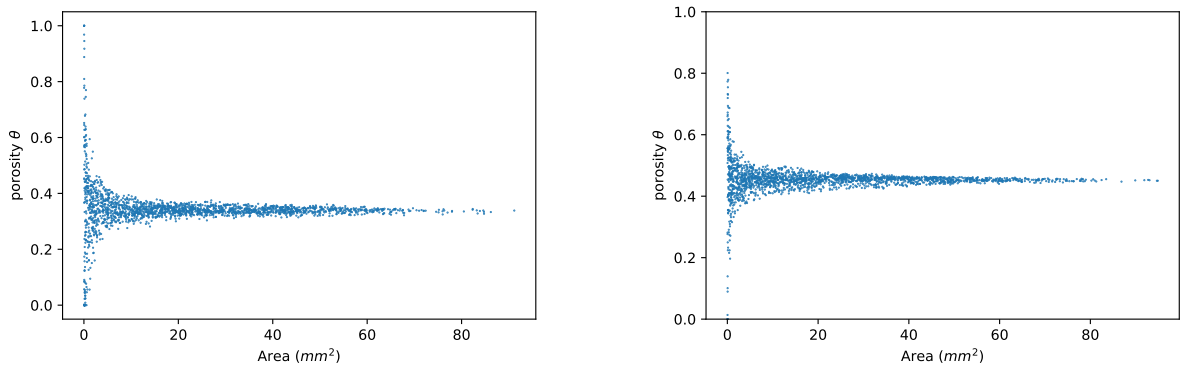


**Figure 10:** *Representative elementary volume (REV) scale test of the generated domains calculated by PoreSpy. Both domains have a total area of 100 $mm^2$. The x-axis is displayed in voxel size, the maximum value of which corresponds to the maximum area of the domain. (a) Analysis of the Homogeneous domain with bigger grains and $\theta = 0.343$. (b) Analysis of the heterogeneous domain with more and smaller grains and $\theta = 0.443$.*

Initially values will oscillate greatly but as the volume of the domain increases, these will dampen out (Fig. 9). Fluctuations at smaller volumes, or below REV, are related to larger influence of individual pore spaces. If the

volume is too large, the domain is no longer considered to be at REV scale, but rather at the field scale [*Brown et al.*, 2000]. Results for REV scale test of the homogeneous and heterogeneous mediums can be found in Fig. 10.

## 2.9 Pore Size Distribution

The pore size distribution was extracted from the domains to further study characteristic parameters describing the porous medium. This was done using the PoreSpy module called local thickness filter. This method is based on research done by *Chiang et al.* [2009]. It iteratively places the largest spheres possible between grains and updates the images (Fig. 11). This process is continued until no more spheres can be placed. The resulting sphere sizes were then stored and plotted as a histogram. Small differences between actual and measured pore size will occur. This is due to the fact that a high quality image, characterized by a small pixel size, had a higher computational time when pixel distance between grains was calculated. Since post-processing of the realizations was not done on the cluster, smaller image sizes were used.

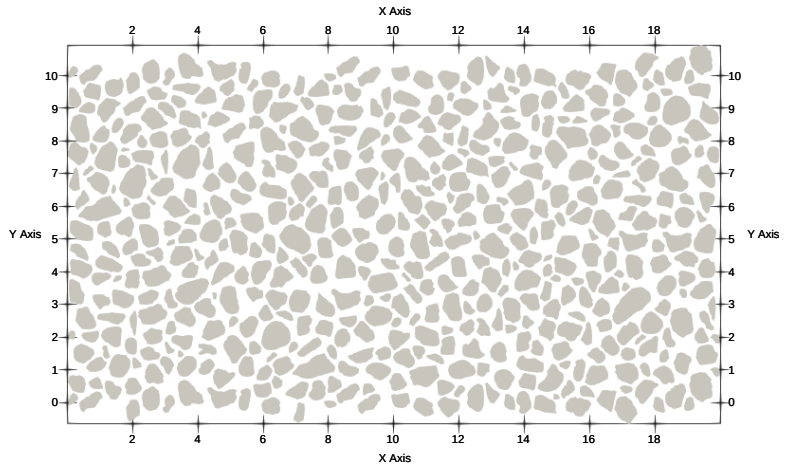


**(a)**

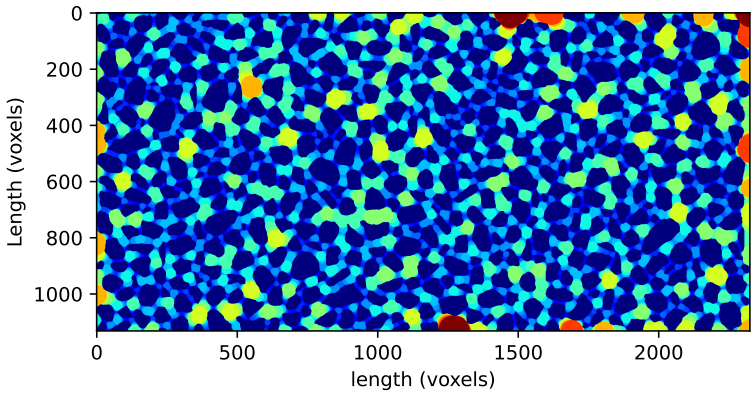


**(b)**

**Figure 11:** *Example domain containing pre-generated grains from microfluidics model (a) with a $\theta$ of 0.465 and the same domain with the applied Porespy filter of local thickness (b).*

## 2.10 Monte Carlo & Convergence Test

The Monte Carlo (MC) method is a computational technique used to determine the uncertainty of a parameter. Multiple realizations being different versions of the model following the same statistical properties, are produced and used as input into a deterministic model [*Lu and Zhang*, 2003]. Output variables of the deterministic model will therefore yield many different values giving rise to a statistical description [*Bear*, 2018]. Here, we employed the MC method by generating a $\theta$ value, grain size and shape distribution and placing the grains within a domain according to a uniform distribution of x and y coordinates. Each MC simulation ensemble will have one porosity value, and a single distribution of grains but realizations with different coordinates. In this case,

the OpenFoam environment is the deterministic model which calculates the permeability value of each specific realization.

The amount of simulation results that are needed were quantitatively analyzed using the method of mean convergence as described in *Ballio and Guadagnini* [2004]. Here simple statistical analysis of the ensemble run results were done using the mean. The mean of the permeability was calculated for the first two simulation results and one by one more permeability values were added (Fig. 12). Initially the mean will oscillate considerably, however as more simulations are performed the oscillation will become smaller. When oscillations have dampened, it can be assumed that enough MC simulations have been executed.

For smaller porosity values, approximately 300 simulations is enough to reach convergence. However, as porosity increases the uncertainty of the permeability increases therefore more simulations were needed to reach convergence. The amount of simulation results varied between approximately 300 and 900 depending on $\theta$ values (Fig. 12).

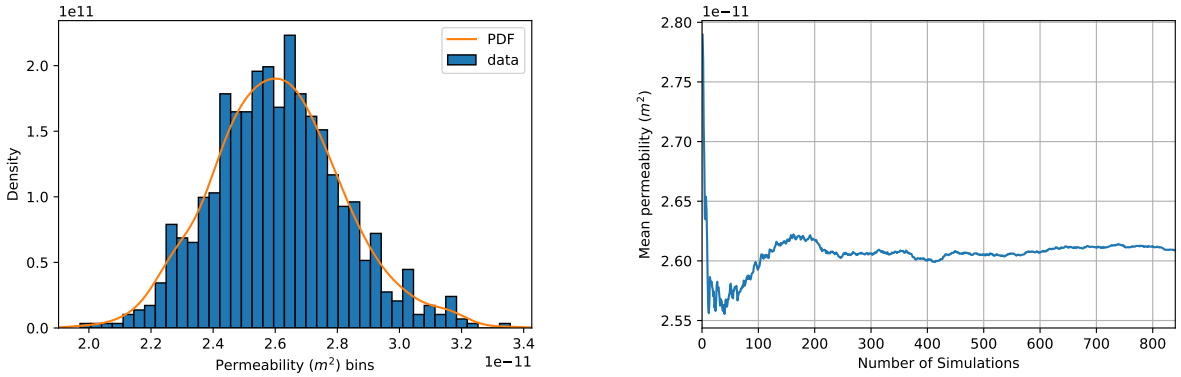


**(a)** **(b)**

**Figure 12:** *(a) Histogram of permeability for a porosity of 0.353 using the same grain sizes and shapes, but different positions. Grain size is obtained from a truncated log-normal distribution with 0.01, 1.0, 0.35, 0.25 for $r_{min}$, $r_{max}$, $r_{mean}$, and $r_{std}$, respectively. (b) Mean permeability of number of simulations plotted for $\theta = 0.336$. Convergence is achieved using approximately 300 simulations.*

## 2.11 Post-processing of Data

After ensemble calculations have finished, the data needed to be processed. This meant removing any porosity and coupled permeability values from the results file from runs that failed. Failure of a model run could occur when placement of a grain failed under low $\theta$ conditions or due to OpenFoam not initiating on the cluster. In general it did not occur often, but failed runs present with a $\theta$ value of 0.999 which will cause incorrect results during statistical analysis.

To remove any outliers, the mean of the porosity was calculated. When running MC on placement, the $\theta$ value was the same for every realization. Therefore, any value that was not equal to this mean was removed from the results file. Empty lines as well as not a number (NaN) data were also removed.

Normality of the data was checked qualitatively using a QQ plot (Fig. 13), and quantitatively using various normality tests. The QQ plot was constructed using the Probplot function taken from the Scipy library [*Virtanen et al.*, 2020] on the permeability data of an ensemble run. If the distribution is normally distributed it will follow a 1:1 ratio between the x and y values. Scipy also enable the use of the Shapiro, Kurtisos, Chisquare, and Jarque-Bera normality tests which provide a quantitative value to describe the distribution. Data for all the MC runs were added to a single file to be plotted as a single porosity vs permeability plot. Using panda dataframe *pandas development team* [2020], the Q1, Q3, interquartile range (IQR), and mean were calculated for each unique $\theta$ value.

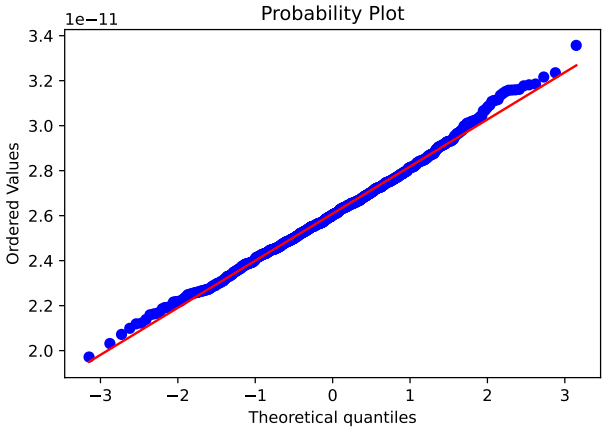


**Figure 13:** *Example QQ plot for a porosity of 0.353 for the "homogeneous" porous domain.*

# 3 Results

The Monte Carlo method was applied to simulate a domain with a fixed $\theta$ and identical grain shapes and sizes but placed randomly within the domain. This was done for different $\theta$ ranges, grain size distributions as well as shapes. The main goal was to built a code that was able to do these types of REV scale simulations as well as be modular. The modularity of the code allows future research applications and ideas to be easily performed. A few scenarios were studied to test the application of the model. The impact of irregularity of shapes compared to spherical grains on the permeability and its uncertainty was studied. The use of porosity-permeability relationships was compared to simulation results to test the applicability at REV-scale.

First, a domain with relatively large grains but narrow cumulative grain size distribution called "homogeneous" was analyzed. Second, a domain with relatively small grains and wide cumulative grain size distribution called "heterogeneous" was analyzed. And lastly a domain containing pre-generated shapes taken from a microfluidics model was analyzed.

## 3.1 Homogeneous: Round vs Irregular

For the homogeneous domains, 52 different porosity values were used along with input parameters of a grain size distribution as described by a truncated log-normal curve. Varying spatial distribution of identical grains within the same domain yielded notable permeability uncertainty (Fig. 14).

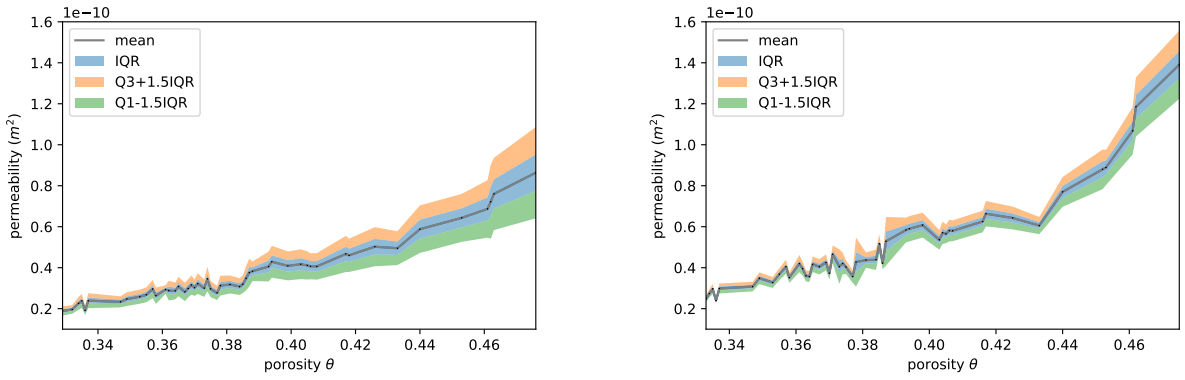


**(a)** *Irregular grains* **(b)** *Circular grains*

**Figure 14:** *Porosity plotted against permeability mean, interquartile range (IQR), where 50% of the density distribution lies, and the outer boundaries, which represent 99.7% of the data, for the homogeneous grain size distribution. Each dot corresponds to a Monte Carlo simulation where porosity and grains are fixed but grain placement is varied. Simulation results of the irregular grains (a) are analyzed in terms of sieve radius and used for circular (b) grains of the same grain size distribution and porosity also varied spatially.*

Permeability as obtained from simulation results and calculated from Darcy's law, shows a similar trend in both irregular (Fig. 14a), and spherical (Fig. 14b) grain domains: increasing permeability with increasing $\theta$. The domains containing spherical grains have in general a higher permeability value as compared to the irregular grain domains generated from the same grain size distribution and $\theta$. Permeability also increases more exponential with $\theta$ in domains containing spherical grains.

The interquartile range (IQR) describes permeability values that fall within the 25th and 75th percentile of the data-set for that porosity. Therefore, if the IQR is larger, permeability values are more spread out and uncertainty is larger. When comparing the irregular and round flow simulation results, the uncertainty of both increase with increasing $\theta$. However, the uncertainty of the irregular domains is significantly larger than that of the spherical domains. Between a $\theta$ of 0.36 and 0.38 the mean permeability fluctuates quite significantly, even more so in the circular grain domains than in the irregular grain domains.

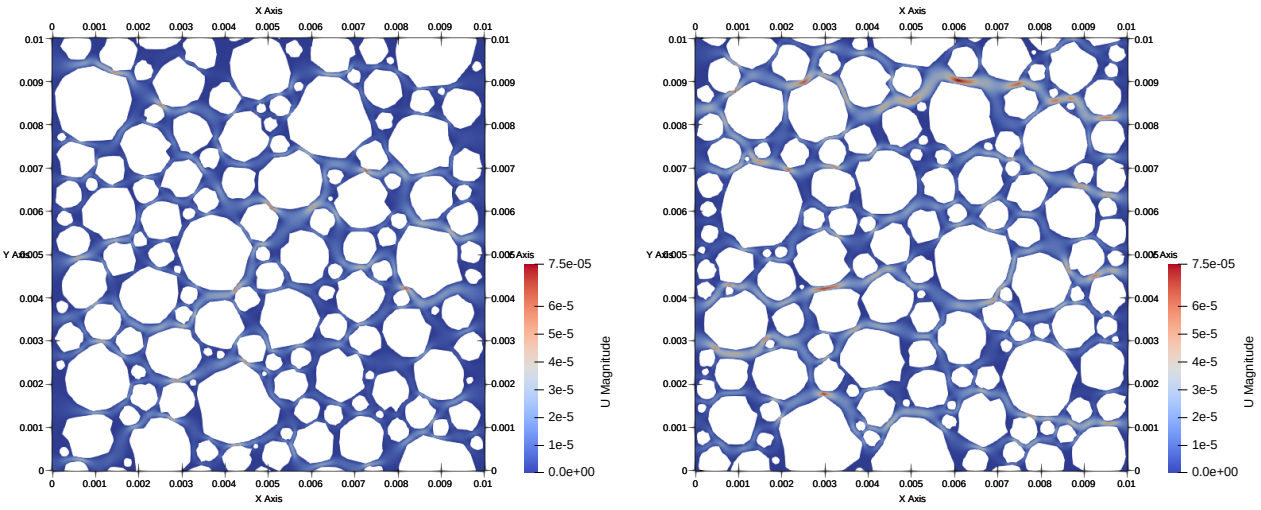


**(a)** *low k* **(b)** *high k*

**Figure 15:** *Two realizations of a homogeneous grain size distribution with a $\theta$ of 0.334. Grains in both realizations are identical in size and shape but vary in spatial placement. Velocity is given in [m/s], length of the domain is given in m, grains are shown in white and flow paths in range of blue to red. These domains are the same as given in appendix A.1 where (a) has the lowest ($1.764e^{-11}m^2$), and (b) has the highest ($2.884e^{-11}m^2$) permeability.*

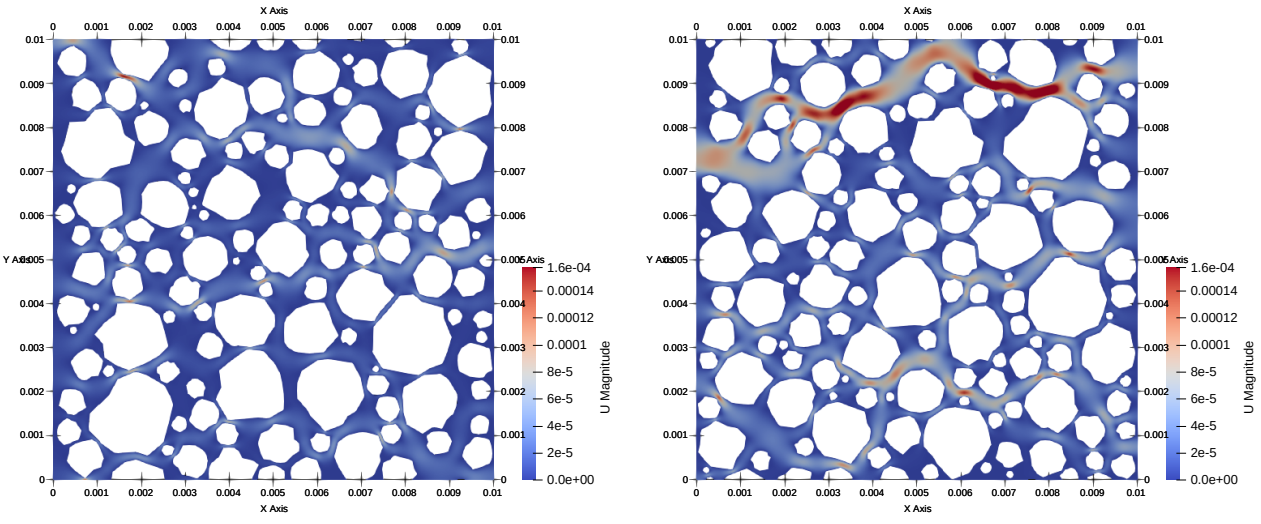


**(a)** *low k* **(b)** *high k*

**Figure 16:** *Two realizations of a homogeneous grain size distribution with a $\theta$ of 0.463. Grains in both realizations are identical in size and shape but vary in spatial placement. Velocity is given in [m/s], length of the domain is given in m, grains are shown in white and flow paths in range of blue to red. (a) has the lowest ($4.791e^{-11}m^2$), and (b) has the highest ($1.110e^{-10}m^2$) permeability.*

The spatial distribution of the grains has an effect on the flow path of the water moving through the pore-space

(Fig. 15 & 16). Permeability as calculated from Darcy's law (Eq. 18) only has one different variable between these two realizations: $u_{mean}$. That means that a higher permeability between two realizations, where all factors were kept constant expect grain positioning, causes a higher the mean velocity. Areas of high flow velocity can be observed. This becomes even more obvious at high porosity (Fig. 16) as can be seen by the much higher maximum flow velocity. The realization with the highest porosity and highest permeability (Fig. 16b) shows a dominant flow path which consists of well-connected large pore sizes.

The pore size distributions as obtained from PoreSpy vary between the two example realizations in Fig. 17a & 17b. The realization with the lowest permeability shows a small amount of smaller pores and a higher amount of larger pores as compared to the realization with the highest permeability. Values seem more closer together with a significant peak around logarithmic value of -0.81 for a higher permeability. Two pore size distributions for a higher $\theta$ of 0.463 were also analyzed (Fig. 17c & 17d). Here permeability values are even farther apart, however grain size distributions do not vary significantly. Average pore sizes for the higher $\theta$ are larger than the domains with low $\theta$.

It should be noted that the minimum distance between grains was set to 0.05mm for both irregular and circular grained domains at the start of the simulation. However, the smallest pore size, as obtained from the Porespy analysis, shows a value of approximately $10^{-1.5}$ = 0,032 mm. This could be caused by the procedure in which the pore sizes are determined not working properly or due to the resolution of the images being too low.

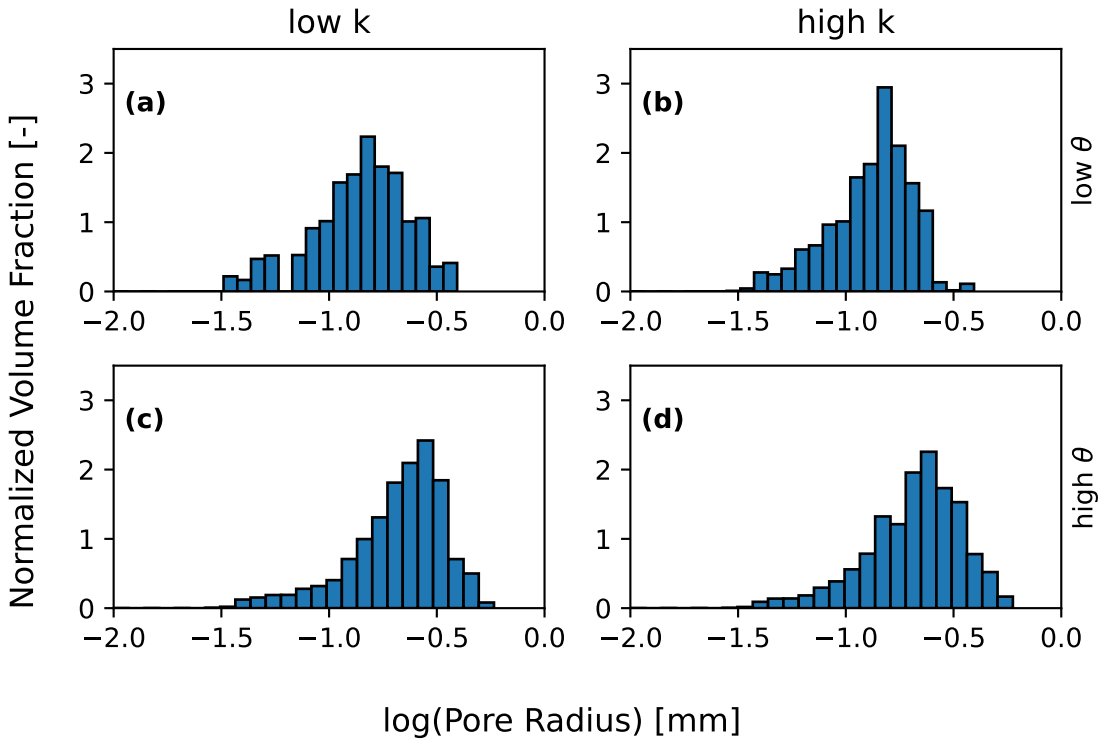


**Figure 17:** *Pore size distributions of different realizations for the homogeneous domains containing irregular grains: (a) $\theta$ = 0.334, $k$ = 1.764$e^{-11}m^2$, (b) $\theta$ = 0.334, $k$ = 2.884$e^{-11}m^2$, (c) $\theta$ = 0.463, $k$ = 4.791$e^{-11}m^2$ , and (d) $\theta$ = 0.463, $k$ = 1.110$e^{-10}m^2$.*

### 3.1.1 Homogeneous: Simulated vs Calculated Permeability

Radii of the irregular grains were determined using the bounding box method (Fig. 4) and plotted as a sieve analysis curve (Fig. 18a). Particle sizes for this simulation type varied between 0.06 and 2 mm in diameter which falls within the specified truncated log-normal distribution input. Differences between distributions were caused by the relatively large grains as compared to the domain size. Therefore, a simulation curve is not a straight line through these points but may vary. The exact curve along with its corresponding $\theta$ are exported and used as input for producing a domain containing spherical grains.

$d_{10}$ is determined from the grain size distribution (Fig. 18b). Diameters ranged between 0.018 and 0.030 mm. Small differences between irregular and circular $d_{10}$ values are caused by taking grains from the grain sieve analysis curve until the exact desired $\theta$ is reached. This might cause more or less grains to be placed than the corresponding irregular domain. Not all simulations were able to reach the exact desired $\theta$. Therefore, they

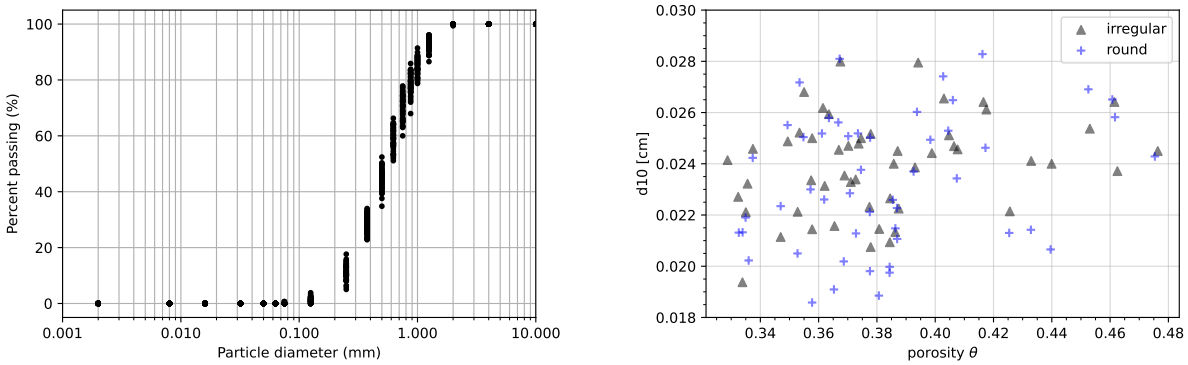


**(a)** **(b)**

**Figure 18:** *Output grain size analysis in terms of sieve diameters using the smallest width method. (a): data points of all the MC simulations that were executed, a single simulation is a line through these points. (b): $d_{10}$ values used to calculate the permeability for the different porosity-permeability relationships plotted alongside its respective $\theta$ for the homogeneous porous media.*

were omitted from the data.

Permeabilities are calculated form emperical relations (Tab. 1) using the obtained $d_{10}$ and $\theta$ values. They are plotted along with the mean permeability of the simulation results (Fig. 19). Slichter (1898), Barr (2001), Hazen (1892), and Beyer (1964) all show relatively good correlation to simulation results for the homogeneous domain. The general trend of increasing permeability with increasing $\theta$ is visible in all relationships with the exception of the Kozeny-Carmen equation. Small fluctuations in permeability from simulation results can also be observed in the permeability as obtained from equations. For example a small decrease in permeability at a $\theta$ of 0.38 can be seen in all relations even the Kozeny-Carman. This same variation can also be noted in the $d_{10}$ values at that $\theta$ (Fig. 18b).

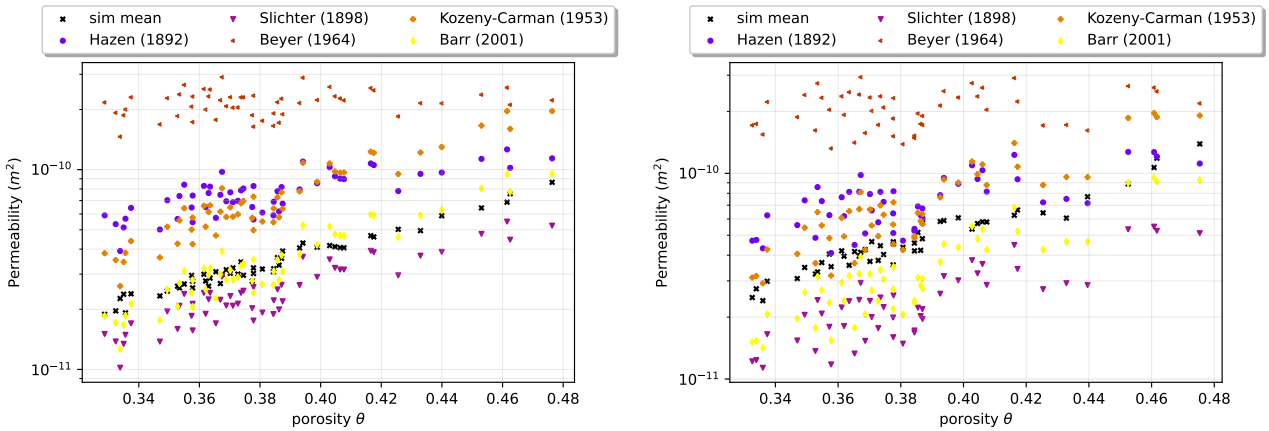


**(a)** *Irregular grains* **(b)** *Circular grains*

**Figure 19:** *Mean permeability of the simulation results plotted with calculated permeability from porosity-permeability relationships against $\theta$ for the homogeneous domain. Permeability is plotted on a log-scale for irregular grains (a) and spherical grains (b). Sieve radii obtained using the bounding box method for the irregular grains are used as input for the spherical grain domains.*

When comparing the permeability values of the irregular (Fig. 19a) and circular (Fig. 19b) domains, it can be seen that while the mean simulation permeability is higher in the circular domains, the porosity-permeability relationships remain approximately similar. Any variation is related to the small differences that exist in the $d_{10}$ value as explained earlier. Since most equations have an exponential relationship between grain size and permeability, a small variation can cause a significant difference.

However, it should be noted that while Barr (2001) shows excellent correlation in the irregular grained domains, it underestimates permeability when simulating circular grains of the same size. Moreover, the predicted permeability of the circular grained domain has a much larger spread of values from the mean.

### 3.1.2 Homogeneous: Grain Shape Parameters

The grain shape parameters, sphericity, roundness, circularity and solidity were calculated for each grain inside a domain. Since every $\theta$ value contains one set of identical grains, as described by shape and size, only 52 domains had to be extracted from the cluster. The grain shape parameters were averaged and plotted against the permeability difference of the spherical and irregular shaped grain domains (Fig. 20). Values varied by approximately 1%. Average values indicate shapes were relatively well-rounded, smooth, and spherical.

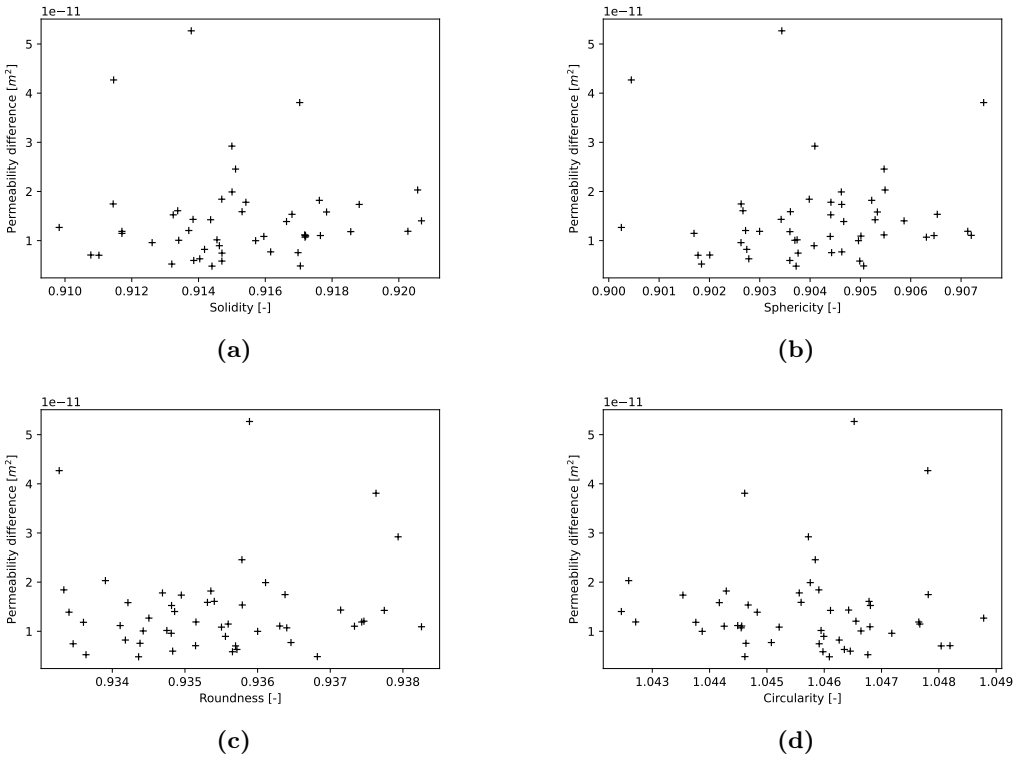


**Figure 20:** *Calculated average shape factors plotted against permeability difference between round and irregular particles using the same grain size distribution for the homogeneous porous media. Plotted quantitative grain shape parameters are: (a) solidity, (b) sphericity, (c) roundness, and (d) circularity.*

No clear relationships between the defined morphological grain parameters and the permeability difference for the homogeneous domains can be observed. Differences between the averaged values will become smaller as the number of grains increases. This is because these grains are generated with the same irregularity parameters. Even though irregular grains have a clear impact on permeability, it cannot be correlated to a quantitative grain shape parameter.

## 3.2 Heterogeneous: Round vs Irregular

For the heterogeneous domains, 27 different porosity values along with the input parameters of a grain size distribution as described by a truncated log-normal curve were used. The same trend that was found in the homogeneous domains can also be seen here: increasing permeability with increasing $\theta$ (Fig. 21). Domains containing round grains generated from the same $\theta$ and grain size distribution (Fig 21b) as the domains containing irregular grains (Fig. 21a) have, in general, a higher mean permeability value. Uncertainty as given by the IQR is increasing with increasing $\theta$. However, uncertainty is smaller when simulating spherical grains. This trend was also observed in the homogeneous domain.

The grain size distribution is the only changed input parameter in the heterogeneous domains as compared to the homogeneous domains. The grain shape parameters, $I$, and $r_v$ are unchanged. Mean homogeneous permeability values are higher than the heterogeneous mean values for the range of overlapping $\theta$. For example, the mean permeability of the homogeneous domain containing irregular grains is approximately $6.410^{-11}m^2$ at a $\theta$ of 0.45. The mean permeability of the heterogeneous domain containing irregular grains is approximately $3.410^{-11}m^2$ at this $\theta$. Uncertainty in the heterogeneous domains is smaller than uncertainty of the homogeneous domains at the same $\theta$. This can be seen by the width of the IQR which is significantly smaller for this grain size distribution.

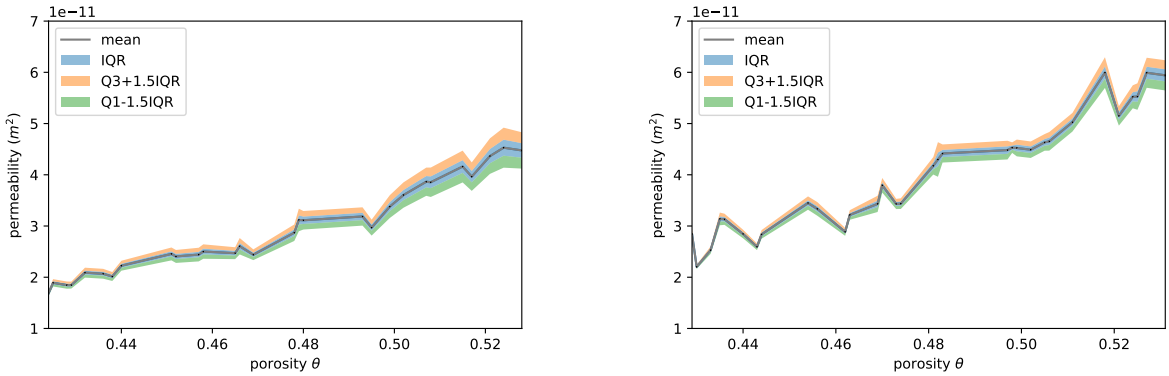


**(a)** *Irregular grains* **(b)** *Circular grains*

**Figure 21:** *$\theta$ plotted against permeability mean, interquartile range (IQR), where 50% of the density distribution lies, and the outer boundaries, which represent 99.7% of the data, for the heterogeneous grain size distribution. Each dot corresponds to a Monte Carlo simulation where $\theta$ and grains are fixed but grain placement is varied. Simulation results of (a) the irregular grains are analyzed in terms of sieve radius and used for (b) circular grains of the same size and $\theta$ also varied spatially.*

Two realizations of the lowest $\theta$, with the lowest and highest $k$ were extracted from the cluster (Fig. 22). The realization with the higher $k$ (Fig. 22b) shows areas with higher flow velocity than the realization with the lowest $k$ (Fig. 22a). The area of higher flow velocities, located at approximately $x = 0.008, y = 0,0035$, shows a preferential flow path unobstructed by grains. Two realizations of the highest $\theta$, with the lowest and highest $k$ were also extracted from the cluster (Fig. 23). Areas of higher flow velocities can also be observed here. Local flow velocities in the realization with the highest permeability (Fig. 23b) are higher as compared to the realization with the lowest permeability (Fig. 23a). The maximum flow velocities in the domains with high porosity are more than double that of the domains with the lower porosity. However, these domains are described by the same grain size distribution and shape parameters.

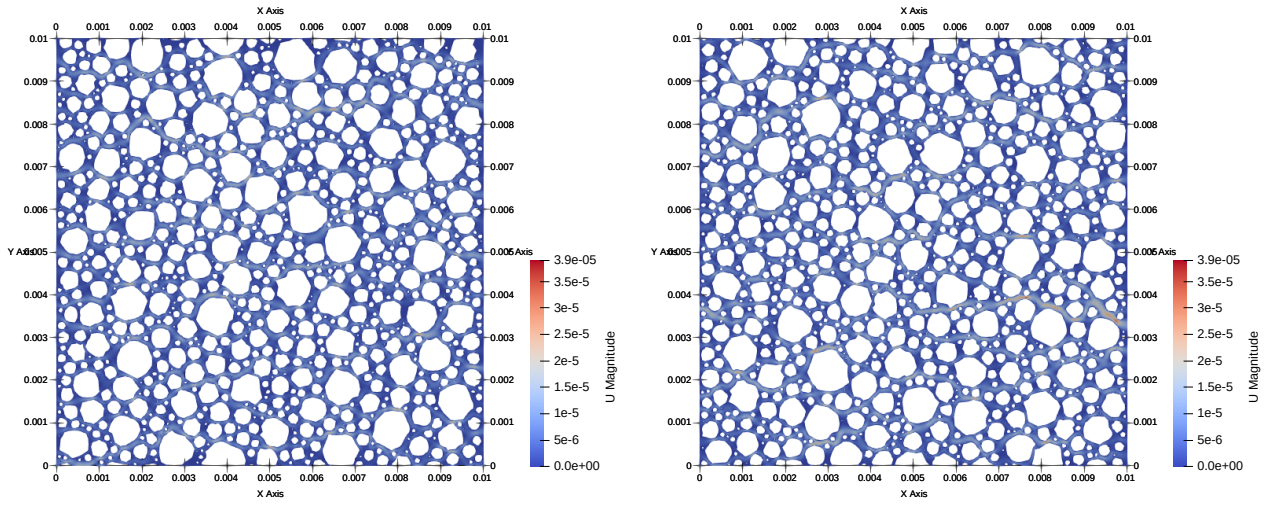


**(a)** *low k* **(b)** *high k*

**Figure 22:** *Two realizations of a porous medium containing irregular grains for a heterogeneous grain size distribution with $\theta = 0.424$. Grains in both realizations are identical in size and shape but vary in spatial placement. Velocity is given in [m/s], length of the domain is given in [m], grains are shown in white and local flow velocities in range of blue to red. (a) has the lowest ($1.595e^{-11}m^2$), and (b) has the highest ($1.794e^{-11}m^2$) permeability.*

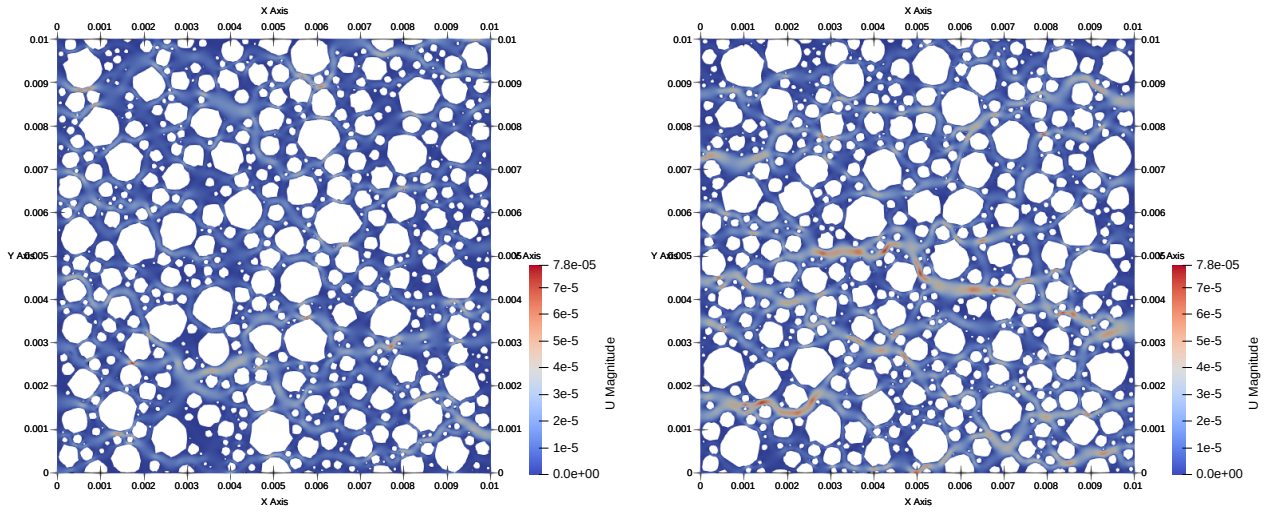


**(a)** *low k* **(b)** *high k*

**Figure 23:** *Two realizations of a porous medium containing irregular grains for a heterogeneous grain size distribution with $\theta = 0.528$. Grains in both realizations are identical in size and shape but vary in spatial placement. Velocity is given in [m/s], length of the domain is given in [m], grains are shown in white and local flow velocities in range of blue to red. These domains are the same as given in Appendix A.3 where (a) has the lowest ($3.766e^{-11}m^2$), and (b) has the highest ($5.290e^{-11}m^2$) permeability.*

Pore size distributions were extracted for the four realizations in fig. 22 & 23 (Fig. 24). The smallest pore size is approximately 0.03 mm, which is smaller than the specified minimum distance between grains. Pore size distributions at low porosity are relatively similar. The peak of the realization with low porosity, high permeability (Fig. 24b) is somewhat higher but at a lower value. The realization with low porosity, low permeability (Fig. 24a) shows a small amount of large pores which cannot be seen for the high permeability realization.

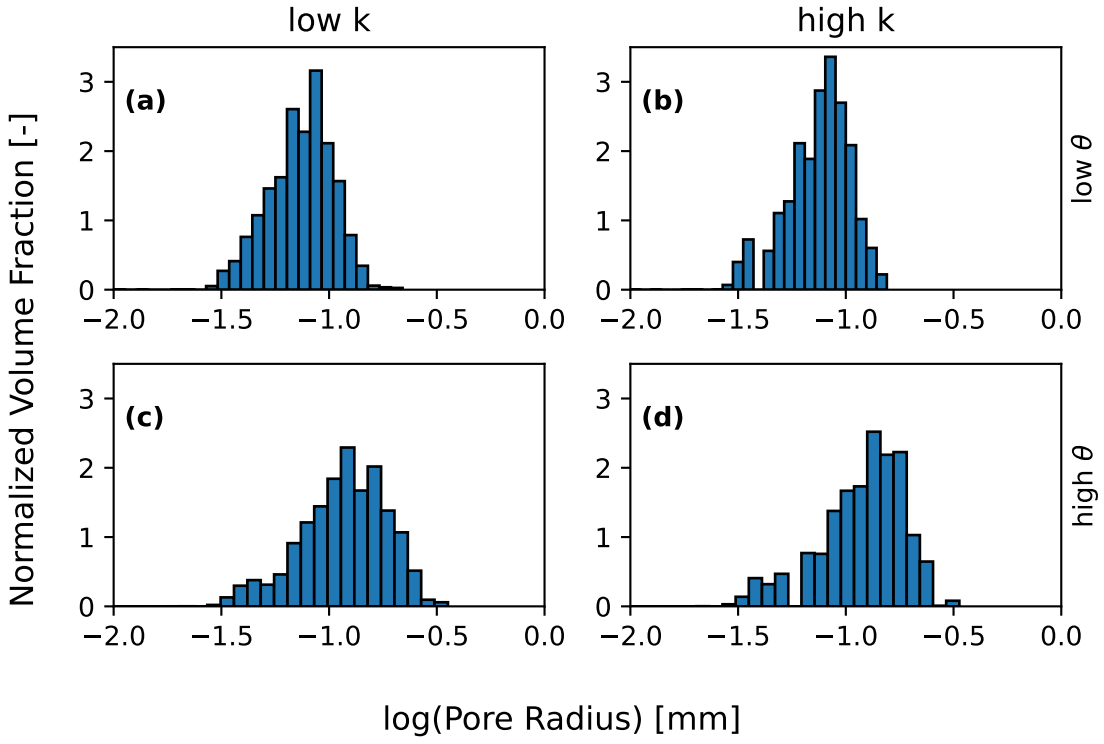


**Figure 24:** *Pore size distributions of different realizations for the heterogeneous domains containing irregular grains: (a) $\theta = 0.424$, $k = 1.595e^{-11}m^2$, (b) $\theta = 0.424$, $k = 1.764e^{-11}m^2$, (c) $\theta = 0.528$, $k = 3.766e^{-11}m^2$, and (d) $\theta = 0.528$, $k = 5.290e^{-11}m^2$.*

The pore size distributions for the high porosity realizations are also quite similar. However, the normalized volume fraction of the realization with the highest permeability (Fig. 24d) is higher at a pore size of approximately $-0.75$ or 0.18 mm. The large pore sizes present in the realization with the lowest permeability for high porosity (Fig. 24c) are not present in the high permeability realization.

The realizations of the high porosity ($\theta = 0.528$) show much larger pore sizes then the realizations of the lower porosity ($\theta = 0424$). This can be seen by the maximum value increasing to approximately $-0.5$ or 0.32 mm. Also the mean of the pore sizes is higher.

### 3.2.1 Heterogeneous: Simulated vs Calculated Permeability

The radii were analyzed using the smallest width method and plotted as a grain size distribution curve in terms of percent passing (Fig. 25a). The distribution curve has a wider range as compared to the homogeneous diameters with values between 0.007 and 1.0 mm. The output grain radii follow the input grain size distribution described by a truncated log-normal distribution with a minimum and maximum radius of 0.001 and 0.5 mm, respectively. The analyzed output radii were used as input for the circular domain generation. This was done to make sure the distribution of the circular domain is the same as that of the irregular domains. The spread of the points in the cumulative grain size distribution is much smaller for the heterogeneous domain than the homogeneous domain (Fig. 18a). This means that populating the domain with more grains minimizes the deviation from the mean that is caused by placing large grains relative to the domain size.

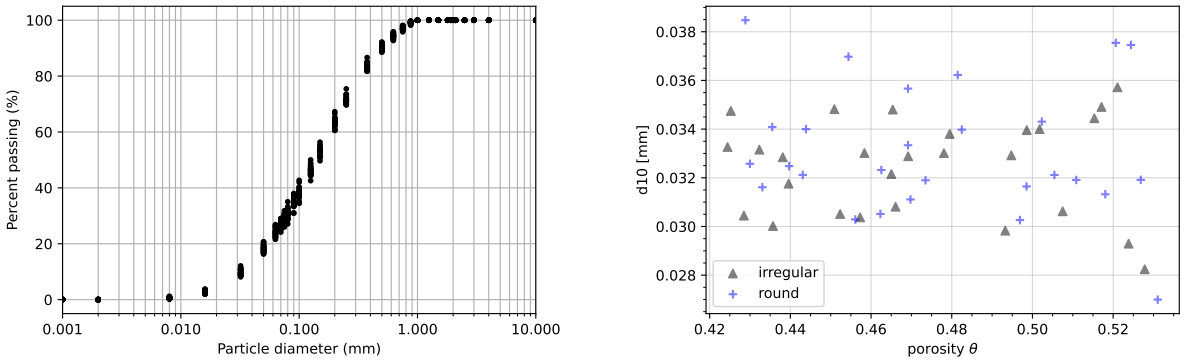


**(a)** **(b)**

**Figure 25:** *(Output grain size analysis in terms of sieve diameters using the smallest width method for the heterogeneous porous media. (a) Data points of all the MC simulations that were executed. A single grain size distribution is composed of points taken from this cumulative frequency plot. (b) $d_{10}$ values used to calculate the permeability for the different porosity-permeability relationships plotted alongside its respective $\theta$.*

The $d_{10}$ values along with its corresponding $\theta$ value were exported and plotted for both the irregular and circular grains for the heterogeneous domain (Fig. 25b). Values ranged between 0.026 and 0.040 mm diameter. Small differences between irregular and circular grains are still present, however deviation is low.

The porosity-permeability equations were solved using the $\theta$ and $d_{10}$ values and plotted alongside the mean of the simulation results (Fig. 26). Increasing permeability with $\theta$ can be observed for both irregular and circular domains for all equations. The trend is, however, less pronounced than that of the homogeneous domain, which has a $d_{10}$ value that is approximately 10 times smaller. Most notable is the fact that the mean simulation results differ by approximately a factor 10 from the calculated values. The uncertainty for the heterogeneous domain is quite small, so the porosity-permeability relationship values do not capture the simulated value well. When looking at the conditions for which these empirical relations can be used, only Barr (2001) can be applied for these $d_{10}$ values.

The porosity-permeability relations all predict the same smaller fluctuations which also capture smaller internal variations in the mean permeability. For example between a $\theta$ range of 0.42 and 0.44, it can be observed that if permeability increases in the mean simulation value, so do the predicted values. For $\theta$ higher than 0.52, the predicted value seems to decrease while the simulated permeability still increases. While mean simulation permeability increases, the calculated permeability values do not increase significantly.

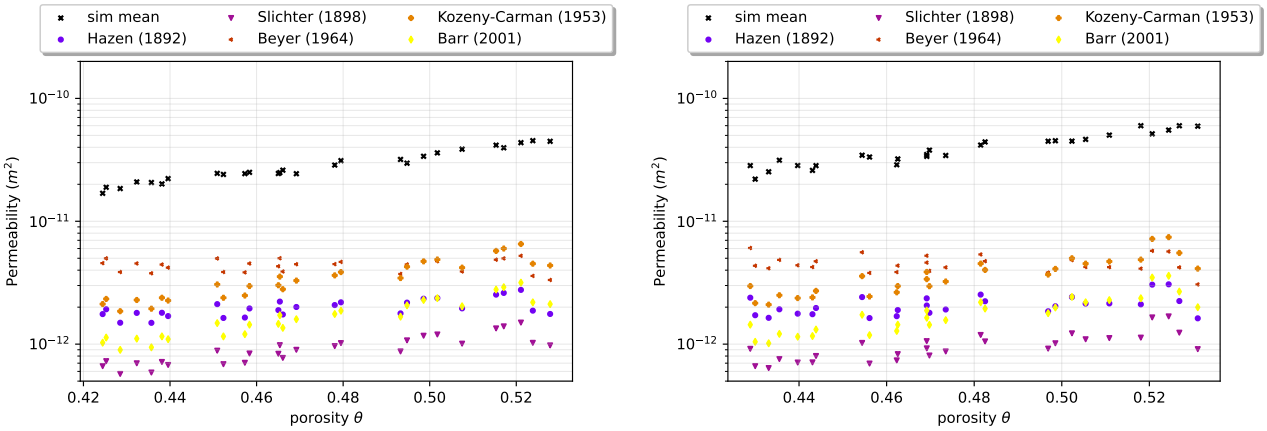


**(a)** *Irregular grains* **(b)** *Circular grains*

**Figure 26:** *Mean permeability of the simulation results plotted with calculated permeability from porosity-permeability relationships against $\theta$ for the heterogeneous domain: for (a) irregular grains and (b) spherical grains. Sieve radii obtained using the bounding box method for the irregular grains are used as input for the spherical grain domains.*

### 3.2.2 Heterogeneous: Grain Shape Parameters

The grain shape factors, sphericity, roundness, circularity and solidity were calculated for each grain inside a domain. Since every porosity value contains one set of identical grains, as described by shape and size, only 27 domains had to be extracted from the cluster. The shape factors were averaged and plotted against the difference in permeability of the spherical and irregular shaped grain domains (Fig. 27). Variations of the mean grain shape parameters were smaller as compared to the homogeneous domains.

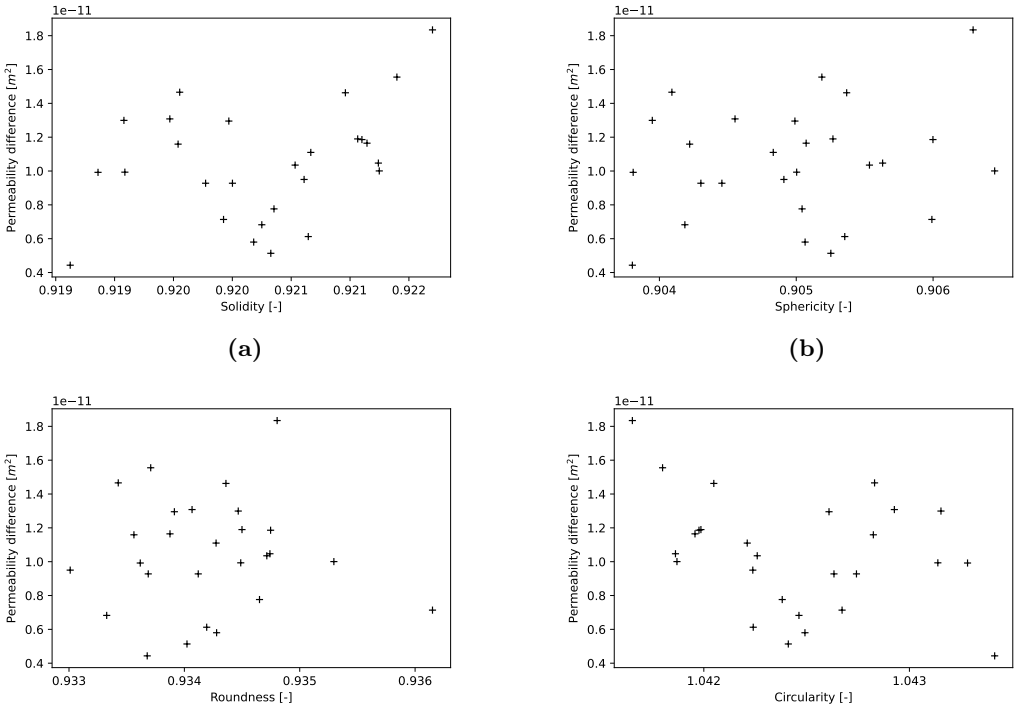


**(a)** **(b)** **(c)** **(d)**

**Figure 27:** *Calculated average shape factors plotted against permeability difference between round and irregular particles using the same grain size distribution for the heterogeneous domains. Plotted quantitative grain shape parameters are: (a) solidity, (b) sphericity, (c) roundness, and (d) circularity.*

No clear relationships between the defined morphological grain parameters and the permeability difference

for the heterogeneous domains can be observed. Since these grains are generated with the same irregularity parameters, differences between the averaged values will become smaller as the number of grains increases.

### 3.3 Pre-generated Grains: Round vs Irregular

For the pre-generated domains, 20 different $\theta$ and grain size distributions were used. These grains were not generated but taken from a file containing grain vertices. These grain vertices were obtained from 2D transformed x-ray tomography data. The simulated $\theta$ range is higher (0.45-0.65) than the other domains. This was done because at lower $\theta$ grains would fail to place causing *theta* variation from the desired input value. However, lower values can be achieved if the minimum distance is reduced. Increasing permeability and uncertainty can be observed with increasing $\theta$ (Fig. 28). Uncertainty is significantly smaller than for the other simulated grain domains. Domains containing circular grains identical in size to the irregular domains according to the sieve radius method (Fig. 28b) showed notably less uncertainty. Permeability shows less fluctuations in mean permeability, but this could be related to the amount of different porosity values simulated.

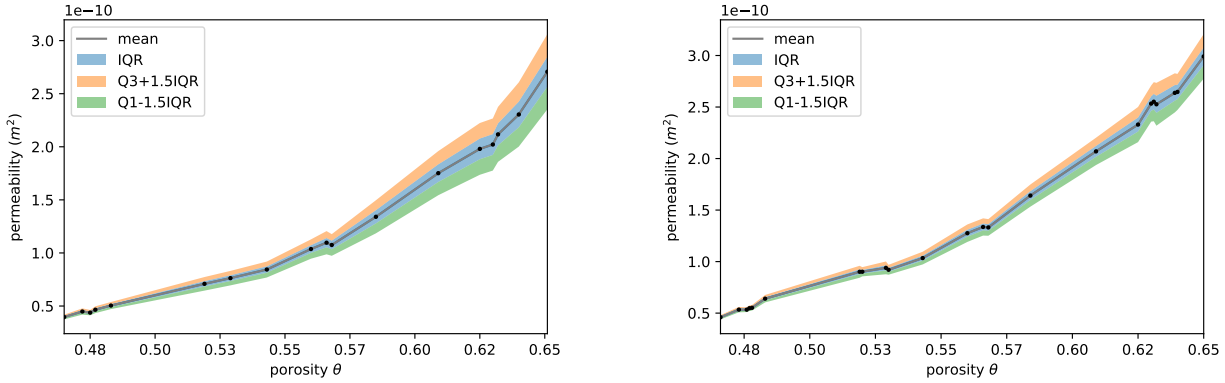


**(a)** *Irregular grains* **(b)** *Circular grains*

**Figure 28:** *Porosity plotted against permeability mean, interquartile range (IQR), where 50% of the density distribution lies, and the outer boundaries, which represent 99.7% of the data, for the pre-generated grain size distribution. Each dot corresponds to a Monte Carlo simulation where porosity and grains are fixed but grain placement is varied. Simulation results of (a) the irregular grains are analyzed in terms of sieve radius and used for (b) circular grains of the same size and porosity also varied spatially.*

Two realizations of a porous medium of $\theta = 0.465$ with internal flow velocities are shown (Fig. 29). While both realizations are identical in grain sizes, shapes and $\theta$, the permeability of (b) is higher than that of (a). Areas of higher flow velocity can be observed within the matrix indicating better connectivity of the pores. Visual inspection of tortuosity yields no significant deviations, further analysis using other methods is required.

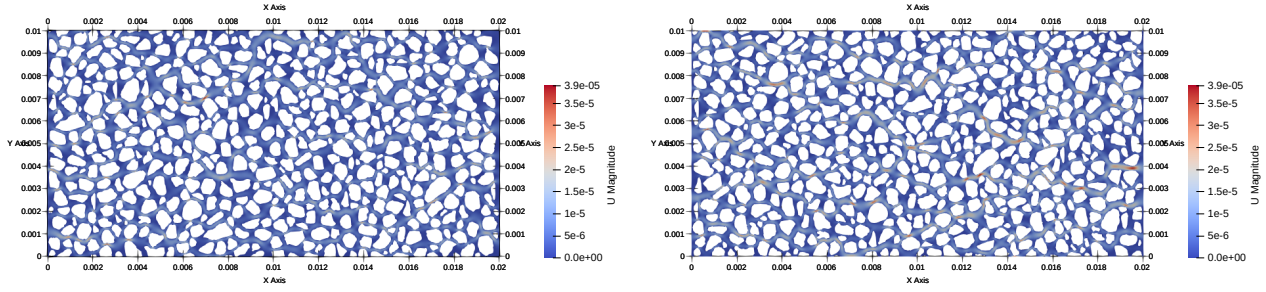


**(a)** *low k* **(b)** *high k*

**Figure 29:** *Two realizations of a porous medium containing pre-generated grains with $\theta = 0.465$. Grains in both realizations are identical in size and shape but vary in spatial placement. Velocity is given in $m/s$, length of the domain is given in $m$, grains are shown in white and flow velocities in range of blue to red. (a) has the lowest ($3.613e^{-11}m^2$), and (b) has the highest ($4.429e^{-11}m^2$) permeability.*

Two realizations of a porous medium of $\theta = 0.651$ with internal flow velocities were also extracted (Fig. 23). Maximum flow velocities are almost 10 times higher than in the low porosity domains. The realization with

the highest permeability (Fig. 23b) shows much better connectiveness of areas with high flow velocities. The realization with the lowest permeability (Fig. 23a) has a significant amount of areas where flow velocities are approximately zero.

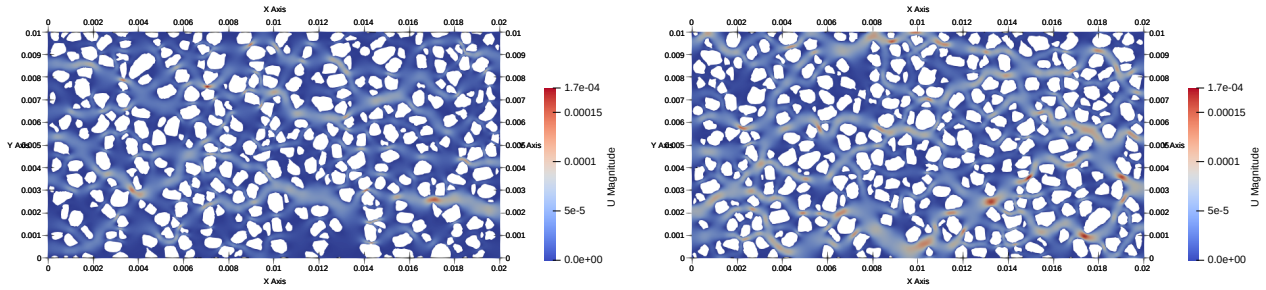


**(a)** *low k* **(b)** *high k*

**Figure 30:** *Two realizations of a porous medium containing pre-generated grains with* $\theta = 0.651$. *Grains in both realizations are identical in size and shape but vary in spatial placement. Velocity is given in* $m/s$, *length of the domain is given in* $m$, *grains are shown in white and flow velocities in range of blue to red. (a) has the lowest (*$2.165e^{-10}m^2$*), and (b) has the highest (*$3.273e^{-10}m^2$*) permeability.*

Two realizations for the lowest $\theta$ (0.465) were used to extract the pore size distributions (Fig. 31). This was done for the realization with the lowest, and the realization with the highest $k$. The same method was applied to two realizations for the highest $\theta$ (0.651). At $\theta = 0.465$, $k$ uncertainty is small and pore size distributions seem relatively similar. The realization with the highest $k$ has overall larger pores as compared to the lower $k$ value. At high $\theta$, uncertainty is significantly larger and grain size distributions differ. The realization with the highest $k$ value has significantly larger pores overall, but relatively the same amount of smaller pores. Comparing the pore size distributions of the low and high $\theta$ domains, it can be observed a higher $\theta$ is correlated to larger pore sizes.

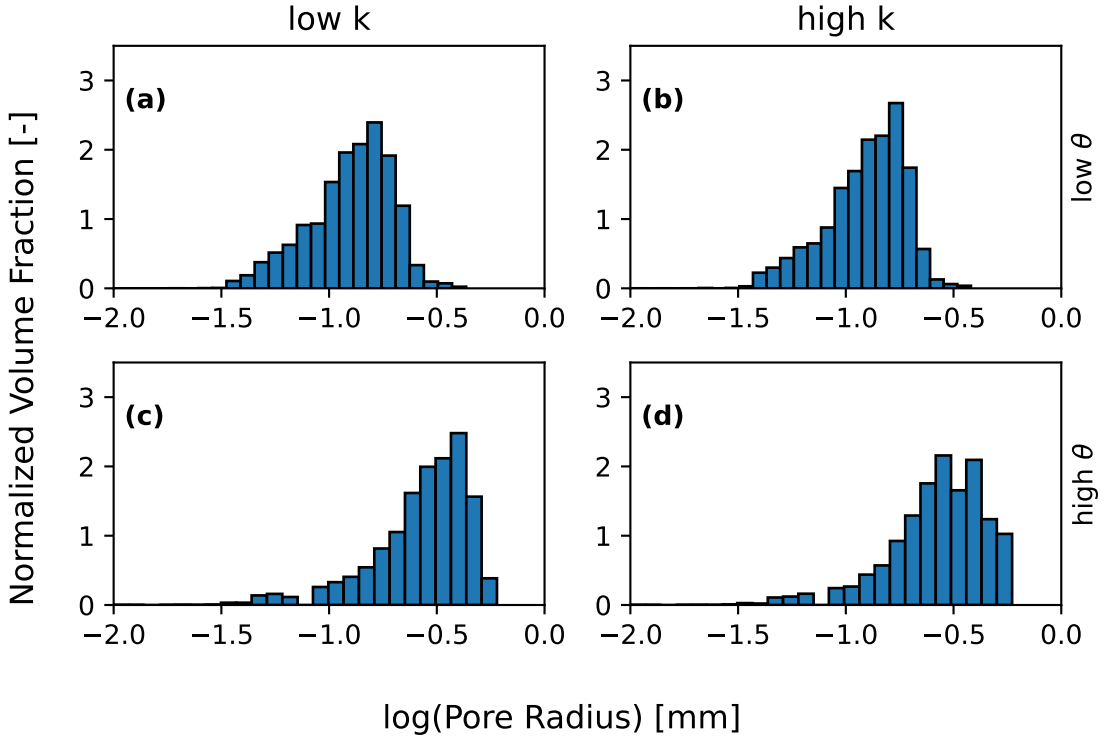


**Figure 31:** *Pore size distribution of different realizations for pre-generated irregular grained domains: (a)* $\theta = 0.4652$, $k = 3.6133e^{-11}m^2$, *(b)* $\theta = 0.4652$, $k = 4.4294e^{-11}m^2$, *(c)* $\theta = 0.6507$, $k = 2.16516e^{-10}m^2$, *and (d)* $\theta = 0.6507$, $k = 3.2734e^{-10}m^2$.

### 3.3.1 Pre-generated: Simulated vs Calculated Permeability

Radii of the grains were analyzed in terms of sieve size and plotted as a grain size distribution (Fig. 32). The curve is significantly smaller than those found in the homogeneous and heterogeneous domains. Particle diameters range between 0.1 and 0.8 mm with the $d_{10}$ being around 0.25 mm, which is almost identical to that of the homogeneous domain. The $d_{10}$ values of the irregular and circular grains are plotted against porosity (Fig. 32b). Small variations between irregular and round $d_{10}$ values can be observed. This is caused by the code trying to obtain the exact porosity value that was set and thus placing the last grain of the size that would yield the same grain size distribution curve. No clear trend can be observed. For some porosity values $d_{10}$ of irregular grain domains is higher while in others the $d_{10}$ of the spherical grain domains.

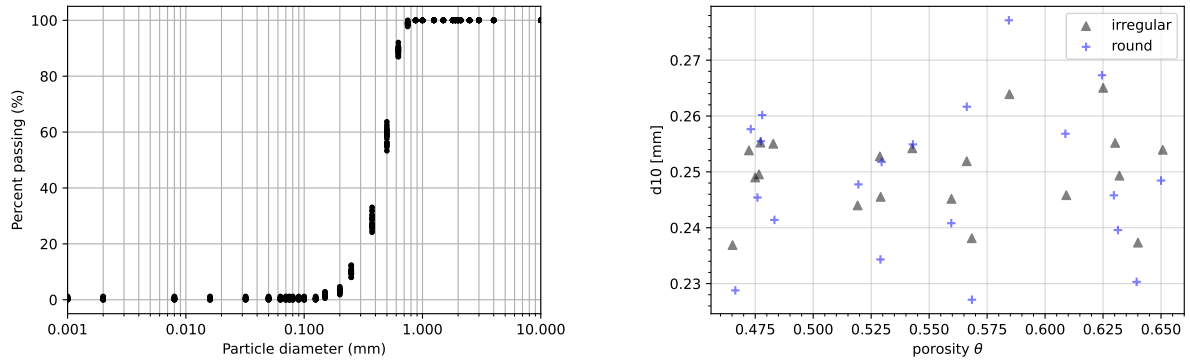


**(a)** **(b)**

**Figure 32:** *Output grain size analysis in terms of sieve diameters using the smallest width method for the pre-generated grained domains. (a) data points of all the MC simulations that were executed. A single grain size distribution is composed of points taken from this cumulative frequency plot. (b) $d_{10}$ values used to calculate the permeability for the different porosity-permeability relationships plotted alongside its respective porosity.*

Empirical and mean simulation $k$ are plotted against $\theta$, with $k$ on a logarithmic and $\theta$ on an arithmetic scale (Fig. 33). A linear relationship between $\theta$ and $\log(k)$ for the empirical relationships and the simulation results can be observed. However, only Kozeny-Carman and Barr seem to correctly capture the effect $\theta$ has on $k$. Slichter shows good correlation between a $\theta$-range of 0.52-0.55, while overestimating $k$ below, and underestimating above this range. Values deviate by a factor 10 for the Kozeny-Carman empirical relationship. Comparison of irregular and round grain domains show that empirical relationships do not capture that mean simulation results increase.

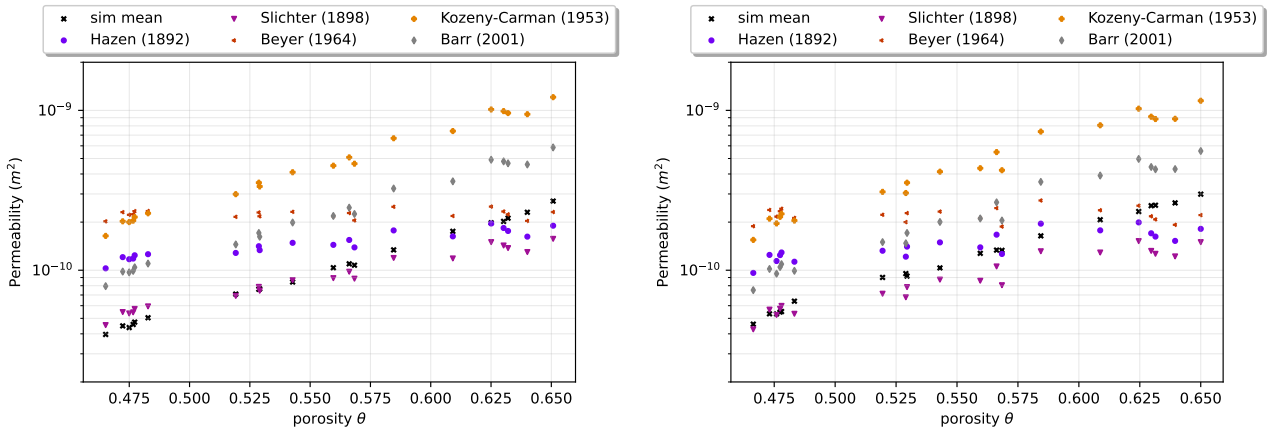


**Figure 33:** *Mean permeability of the simulation results plotted with calculated permeability from porosity-permeability relationships against porosity for the pre-generated grained domain: (a) irregular grains, and (b) spherical grains. Sieve radii obtained using the bounding box method for the irregular grains are used as input for the spherical grain domains.*

### 3.3.2 Pre-generated: Grain Shape Parameters

Shape factors were calculated for each grain and the average was plotted against the difference between irregular and round mean permeability result (Fig. 34). Average shape factors varied more than as compared to the heterogeneous and homogeneous domains but were still relatively similar. No clear trend for sphericity, roundness or circularity could be observed.

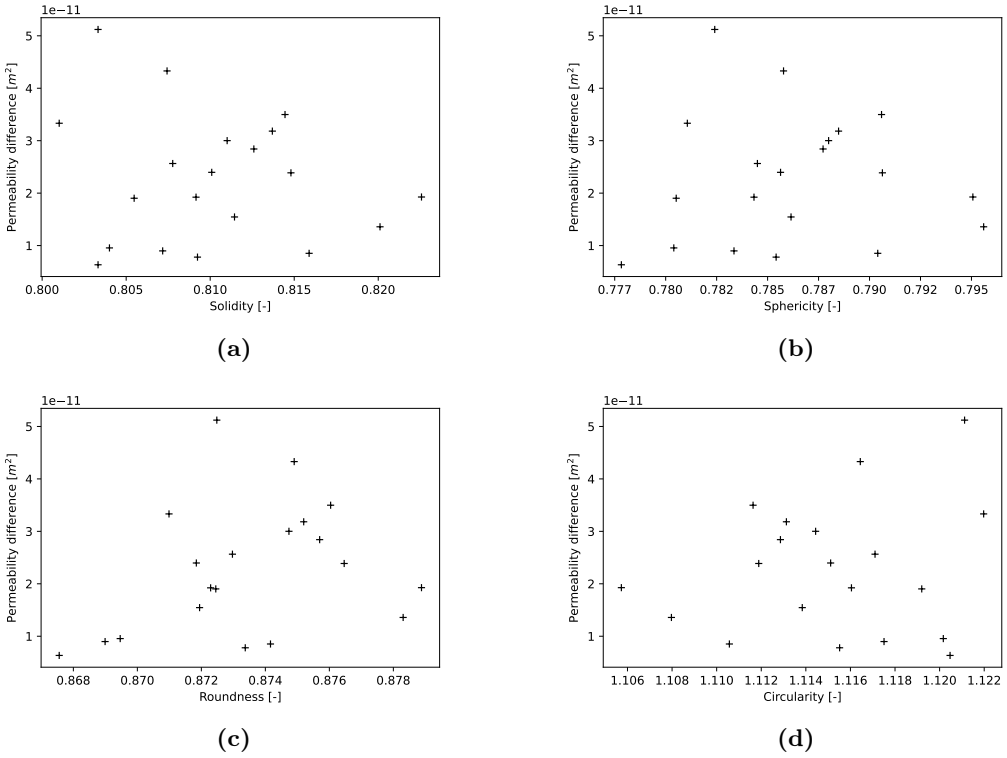


**Figure 34:** *Calculated average shape factors plotted against permeability difference between round and irregular particles using the same grain size distribution for the pre-generated grained domains. Plotted quantitative grain shapes are: (a) shape factor 1, (b) sphericity, (c) roundness, and (d) circularity.*

## 3.4 Comparison of the Domains

Regression lines are plotted through the mean simulation $k$ for the different domains and grain shapes (Fig. 35). This was done to compare the effect of different grain size distributions on $k$. It can be observed that the increase of $k$ with $\theta$ is slightly lower for the heterogeneous domains. Mean $k$ results overlap for the $\theta$ range of approximately 0.46-0.47. Here, the lowest permeability can be observed in the order: heterogeneous, pre-generated, and homogeneous domains. The main difference between the heterogeneous and homogeneous domain is the grain size distribution. Their grains are both generated using the same irregularity parameters, but the homogeneous domain contains considerably more smaller grains. It should be noted that we assume the trend line continues in the same matter above and below simulation results. Comparison of the domains over this rather small $\theta$ range might not be representative for other porosity values. Overall circular grained domain simulations yield higher results when compared to grain size distributions of identical size but irregularly shaped. Average $d_{10}$ values were approximately 0.24, 0.033, 0.25 mm for the homogeneous, heterogeneous and pre-generated domains respectively.

Pore sizes for the heterogeneous realizations were relatively small as compared to the homogeneous and pre-generated realizations. The largest pore size for low porosity being approximately $10^{-0.75}$ mm and high porosity approximately $10^{-0.5}$ mm. For the homogeneous and pre-generated realizations this was $10^{-0.5}$ mm for low porosity and $10^{-0.25}$ mm for high porosity.

In general, pore size distributions for low porosity were relatively similar with small variations between the realizations of high and low permeability. At high porosity, where the permeability difference between realizations is larger, pore sizes were also relatively similar. However, pore sizes at high porosity were much larger. The heterogeneous domains showed much smaller pore sizes as compared to the homogeneous domain. The distribution of the pore sizes was also much narrower for the heterogeneous domain.

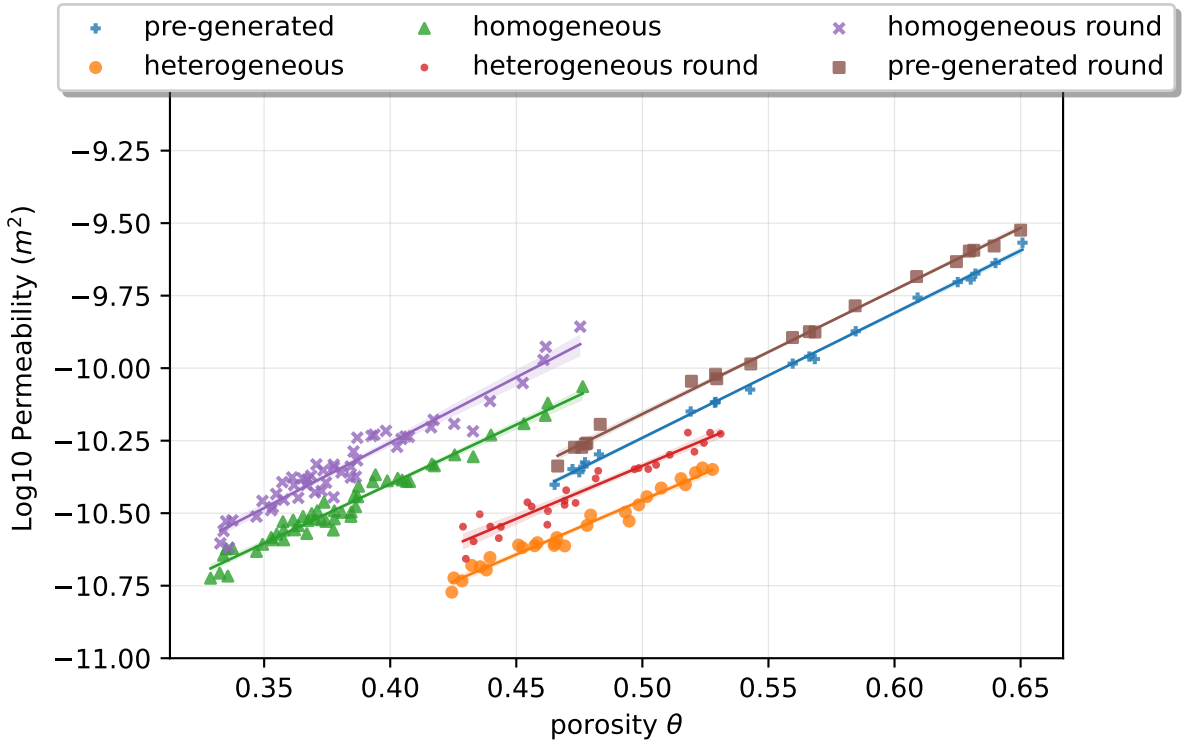


**Figure 35:** *Mean simulation permeability values plotted for the irregular and circular grained domains. Regression lines are plotted for each of the different grain size distributions: homogeneous, heterogeneous and pre-generated.*

While the pre-generated domain and the homogeneous domain have approximately identical $d_{10}$ values, their respective $k$ values differ. From these simulation results, it can clearly be observed that the grain size distribution and grain shapes have an impact on the permeability which is underrepresented in the empirical relationships.

# 4 Discussion

## 4.1 Porosity vs Permeability

Permeability is a measure of the ability of a medium to transport water and is directly related to the connectiveness and size of the pores. The size of pore bodies and throats becomes larger as porosity increases. Therefore, increasing permeability with porosity was expected. An exponential relation between porosity and permeability has already been shown by experimental research [*Chilingar*, 1964; *Chierici*, 2013]. This exponential relation has also been shown here in the mean permeability of the simulation results for all grain size distributions. Differences in permeability caused by the grain size distribution could be observed. However, realizations of porous media described by the same porosity and grain size distribution showed different permeability values as well.

Pore size distributions were relatively similar at low and high porosity. However, permeability uncertainty at low porosity was small as compared to high porosity. According to the law of Hagen–Poiseuille, the permeability is related to the square of the effective radius of the pore size [*Nimmo*, 2013]. *Marshall* [1957] showed that larger pores have an even bigger impact than the squared value of the radius. Thus, having larger pores results in higher permeability. Here, we showed that the larger pore sizes could be found with higher porosity. Small differences in pore size distributions between realizations were found but not significant. This means that the pore size distribution is not the controlling factor causing the large permeability uncertainty at high porosity. We suggest that the connectiveness of the pores is not taken into account. It could be observed that large pores connected with each other caused the highest permeability. Due to the specified distance between the grains, all pores are connected but flow in the x-direction might not be favorable in vertical pore throats. This was observed for the pre-generated realizations at high porosity. A large amount of areas with almost no flow could be observed at low permeability.

It could also be observed that realizations of high porosity showed more straight flow paths. Previous research

has shown that a tortuosity decrease is correlated to a porosity increase [*Matyka et al.*, 2008]. However, our results indicate some other factor controlling the tortuosity of the system: spatial distribution. Higher permeability uncertainty at high porosity can also be explained by tortuosity and grain placement. Since the pore size distributions are almost identical, the variation of values cannot be caused by this. Tortuosity at high porosity is low, which allows water flow in the x-direction to move more freely and have thus higher velocities. Any obstacle placed on that flow path would have a high impact on the distance travelled and cause lower permeability values.

This also explains the smaller uncertainty for circular grains as compared to irregular grains: because water moving around an irregular shape, which has a rough surface, would have to deviate from the flow path significantly more than when moving around a circular grain of the same size. As grains become smaller in the heterogeneous domain, this effect also becomes smaller. Further research on the tortuosity of the domains is necessary to confirm this hypothesis. A method stated by *Graczyk and Matyka* [2020] allows the calculation of the tortuosity from the velocity vector field which can be extracted from the generated VTK file. It uses the average magnitude of the fluid velocity and the average of its component along the macroscopic direction of the flow.

The impact of $\theta$ on permeability has been validated based on only three grain size distributions. Future research could focus on fixing porosity and altering the grain size distribution to observe whether the behaviour is correctly captured by the porosity-permeability relationships.

## 4.2 Porosity-Permeability Relationships

Porosity-permeability relations show the same exponential trend as the simulation results. However, the values between the different relations varied and generally were not able to exactly capture the mean of the simulations. The estimated permeability values varied by more than a factor 10 for the heterogeneous domain. While most of the conditions for the empirical relations were not met, Barr (2001) should have been applicable. A similar trend of underestimating the permeability for smaller grain sizes was found by *Živković et al.* [2021] through experimental analysis of different samples. They also state that as grain sizes increase, and the fraction of smaller sized grains decreases, the permeability increases. This was also observed in this research, however a more extensive analysis of different grain size distributions could improve this view. Experimental research into the relation between grain size, grain shape, grain sorting, porosity and its relative impact on permeability done by *Beard and Weyl* [1973] found a similar relationship. They found a decrease in permeability when grains became finer and sorting became poorer.

We used the relationships defined by *Devlin* [2015] based on the effective grain size value of $d_{10}$. There has been some debate about whether usage of the $d_{10}$ in porosity-permeability relationships was originally intended by the authors [*Urumović and Urumović*, 2017, 2018]. The problem is that no clear definition of the "effective grain size" exists, and different interpretations have been given. For example some use the harmonic mean while other calculate the median of the grain sizes. Further correlation could be done in future research to find the grain size parameters which best suit the data.

Another aspect to consider is the uncertainty shown here. Realizations of the same porosity and grain size distribution showed a range of different permeability values. However, the empirical relations only estimate a single value. This can be attributed to the fact that empirical relationships such as the Kozeny-Carman or Barr ignore microscopic porous medium properties such as pore size distribution, connectivity of pores and spatial distribution and therefore cannot accurately describe the permeability [*Chen et al.*, 2020].

## 4.3 Grain Shapes

No correlation between the proposed quantitative grain shape parameters and permeability difference between irregular grained domains and circular grained domains was found. However, a clear permeability difference caused by irregular grains was observed. *Safari et al.* [2021] modelled porous media using the discrete element method. They found that as grains deviated from a spherical shape, the permeability increased due to the formation of large pore spaces in the domain. A similar study as done here was done by *Liu and Jeng* [2019]. They analysed the relation between morphological parameters, such as roundness and sphericity, to the permeability as calculated from the Kozeny-Carman equation. Results showed increasing permeability as shapes became more spherical and round.

The lack of correlation between permeability difference of irregular and circular grained domains could be related to multiple causes. The irregular shaped grains are generated using the radius variance, and irregularity input parameters. To obtain a relationship between porosity and permeability, these parameters were not varied.

Therefore, the difference in quantitative grain shape parameters between grains were small. Differences will become even smaller when averaging these parameters for a given domain. Especially if the number of grains is very large. Thus, a better method would be to either vary the input parameters for irregular grain shape generation, or use multiple moments to describe the distribution of grain shape parameters. A recommendation for future research is to fix porosity and the grain size distribution, but vary the irregularity, radius variance, and number of vertex points parameters for the generation of irregular grains similar to the work of *Liu and Jeng* [2019].

### 4.4 Recommendations & Future research

While a number of different possibilities of our model were demonstrated here, a large number of questions and ideas can still be formulated and computational improvements made. For example while the relationship between porosity and permeability has clearly been shown here, the impact of grain size distribution is somewhat underrepresented. It is possible to fix the porosity, but generate different grain size distributions which would allow a more detailed analysis. This could also be done for the analysis of the impact of grain shapes: fix the porosity and grain size distribution but alter the irregularity parameters. In this study, a number of experimental data sets have been referenced, each with porosity, permeability and grain size data. Uncertainty analysis of permeability and subsequent comparison to lab measurements could provide valuable insight into the use of our model to predict permeability instead of using the empirical relations.

Due to the modularity of the code, other empirical relationships, different methods of grain generation, grain placement, and grain analysis can be added easily. Other parameters which exist in the original Kozeny-Carman relation, such as the specific surface area of the grains, can be extracted from the domain with relative ease. Often this is done experimentally through porosimetry or gas absorption methods *Sibiryakov et al.* [2021].

Methods of grain placement can be implemented to reduce computational time and possibly improve computations. For instance a watershed type method could be implemented. Currently, grains are placed randomly within the domain and overlap with other grains is checked until no overlap occurs. A better method is extracting the distance between the currently placed grain and fitting a grain of desired size in that available space. This would yield lower porosity values allowing further analysis of porosity-permeability relationships. Also the use of field data to represent grain size distributions could prove useful. This would yield a more asymmetric cumulative grain size curve, representative of an actual grain sieve analysis. The pre-generated domains can be validated by microfluidics experiment by simulating fluid and colloid transport within a realization.

A number of different pore size distributions were shown here. However, these only showed the distributions at low and high porosity for the lowest and highest permeability. To show the relation between permeability and the pore size distributions more clearly, the moments of distribution could be extracted.

## 5 Summary and Conclusions

The main goal of the research was to develop a modular python workflow for the generation and analysis of different porous media. A few scenarios were investigated to test the applicability of our model. The permeability uncertainty that comes from placement of identical grains within a medium was analyzed and compared to permeability-porosity equations. The permeability difference between porous media containing circular and irregular shaped grains was analysed. This was done for domains with the same porosity and grain size distribution but different grain shapes. Properties of the porous media, such as pore size distribution and local flow velocities, were extracted.

The results showed that permeability increased with porosity. This was attributed to increasing pore sizes. Uncertainty between realizations of the identical porosity and grains was caused by connectivity of areas of high flow velocity, but this was most likely not the only cause. The size of the grains also had a clear impact on permeability. Grain size distributions containing smaller grains caused smaller uncertainty. No relationship was found between grain morphology parameters and permeability difference. However, circular grained domains showed significantly higher permeability than irregular grained domains with the same grain size distribution and porosity. This is most likely caused by smaller tortuosity for the circular grains of the same size, but more research is necessary to confirm this hypothesis. The uncertainty at the same porosity was smaller for the different domains. In order of largest to smallest uncertainty at the same porosity: irregular homogeneous, round homogeneous, irregular heterogeneous, and round heterogeneous domains. Comparing the results to known permeability-porosity values showed good capture of the impact of porosity for Kozeny-Carman, Barr, and Slichter, but underestimation of the impact of grain size distributions. While most empirical relations captured the impact of porosity on permeability, correlation between values of numerical simulations was poor,

with variations over a factor of 10. Empirical permeability relationships often oversimplify the fluid transport in porous media. While porosity and grain size distribution have an impact on permeability, pore scale properties such as pore size distribution, tortuosity, and grain morphology are not always considered.

Our results lead us to the major conclusions:

- A grain size distribution which contains more smaller grains has a lower permeability caused by smaller pore sizes.
- Spatial arrangement of grains can cause areas of low flow velocity to form and affects the connectivity of the larger pores thus influencing permeability.
- While grain irregularity decreases the permeability, a relationship between defined morphological parameters could not be found. Further research where porosity is fixed, but grain shape parameters are varied is necessary. This can easily be achieved due to the modularity of this porous medium generator.
- Permeability uncertainty increases as pore sizes increase, grain sizes become larger, and sorting poorer. More grain size distributions are necessary for further study.
- Porosity and effective grain size are not enough to describe the complexity of the porous medium structures. Using these variables in empirical permeability relations will yield a single value while numerous structures can be described by them.

# Declarations

**Conflicts of interests:** The author declares that the research was conducted in the absence of any commercial or financial relationships that could be construed as a potential conflict of interest.

**Availability of data and code:** Manuscript data and codes are included as electronic supplementary material.

# Appendix

## A Realizations of grain size distributions

This section contains different realizations of porous media containing identical grains but with different spatial arrangement. The realization with the highest and lowest permeability value are displayed. Porous media containing irregular grains as well as porous media containing circular grains obtained from the sieve analysis method are shown. Some images are generated using truncated log-normal distributions, described by parameters: $r_{\min}$, $r_{\max}$, $r_{\text{mean}}$, and $r_{\text{std}}$, while others are generated using grains from a pre-generated list. Irregular grained settings are kept constant at 0.5, 0.08, 15 for angular spacing, radius variance, and number of shape points, respectively.

- Fig. A.1: Homogeneous, irregular, 0.01, 1.0, 0.35, 0.25 for $r_{\min}$, $r_{\max}$, $r_{\text{mean}}$, and $r_{\text{std}}$, respectively. Both figures have a $\theta$ of 0.334. Fig. A.1a has the lowest permeability value ($1.764e^{-11}m^2$) of this Monte Carlo simulation, while Fig. A.1b has the highest permeability value ($2.884e^{-11}m^2$).
- Fig. A.2: Homogeneous, round, radii obtained from sieve radius analysis. Both images have a $\theta$ of 0.334. Fig. A.2a has the lowest permeability value ($2.379e^{-11}m^2$), while Fig. A.2b has the highest permeability value ($3.036e^{-11}m^2$).
- Fig. A.3: Heterogeneous, irregular, 0.01, 0.6, 0.45, 0.005 for $r_{\min}$, $r_{\max}$, $r_{\text{mean}}$, and $r_{\text{std}}$, respectively. Both figures have a $\theta$ of 0.424. Fig. A.3a has the lowest permeability value ($1.595^{-11}m^2$) of this Monte Carlo simulation, while Fig. A.3b has the highest permeability value ($1.794e^{-11}m^2$).
- Fig. A.4: Heterogeneous, round, radii obtained from sieve radius analysis. Both images have a $\theta$ of 0.424. Fig. A.4a has the lowest permeability value ($2.655e^{-11}m^2$), while Fig. A.4b has the highest permeability value ($3.052e^{-11}m^2$).
- Fig. A.5: Pre-generated, irregular, porosity and permeability values are: $\theta = 0.651$ (A.5a),(A.5b) and $k = 2.165e^{-10}m^2$ (A.5a), $3.273e^{-10}m^2$ (A.5b) $\theta = 0.4664$ (A.5c), (A.5d) and $k = 3.613e^{-11}m^2$ (A.5c), $4.429e^{-11}m^2$ (A.5d).
- Fig. A.6: Pre-generated, irregular, porosity and permeability values are: $\theta = 0.650$ (A.6a),(A.5b) and $k = 2.644e^{-10}m^2$ (A.6a), $3.380e^{-10}m^2$ (A.6b) $\theta = 0.4652$ (A.6c), (A.6d) and $k = 4.304e^{-11}m^2$ (A.6c), $5.005e^{-11}m^2$ (A.6d).

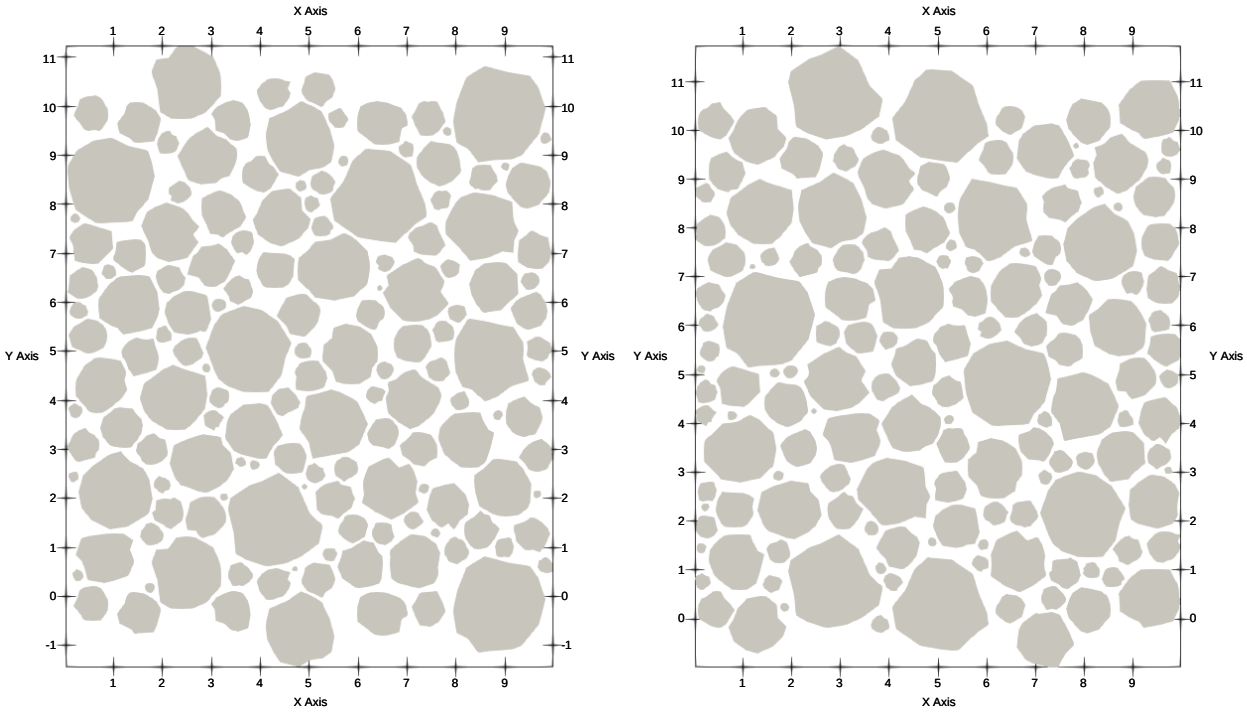


**Figure A.1:** *Two pore-scale domains containing randomly generated irregularly shaped grains but placed at different positions. The grain size distribution is generated using a truncated log-normal grain size distribution with values: 0.01, 1.0, 0.35, 0.25 for* $r_{min}$, $r_{max}$, $r_{mean}$, *and* $r_{std}$, *respectively. Settings for irregular grain parameters are set to: 0.5, 0.08, 15 for angular spacing, radius variance, and number of shape points, respectively.* $\theta$ *of these images is 0.334, with (a) has the lowest permeability value (*$1.764e^{-11}m^2$*) of this Monte Carlo simulation, while (b) has the lowest permeability value (*$2.884e^{-11}m^2$*). Cyclicity of the grains can be seen. Domain length and height are given in mm*

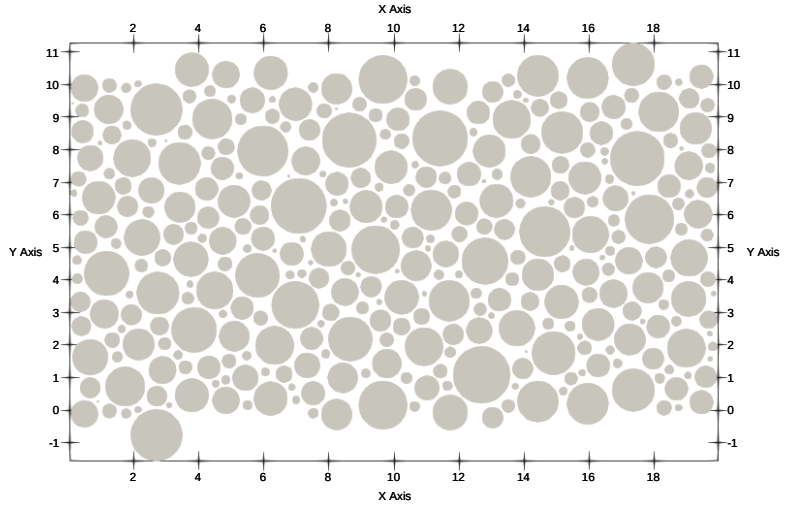


**(a)**

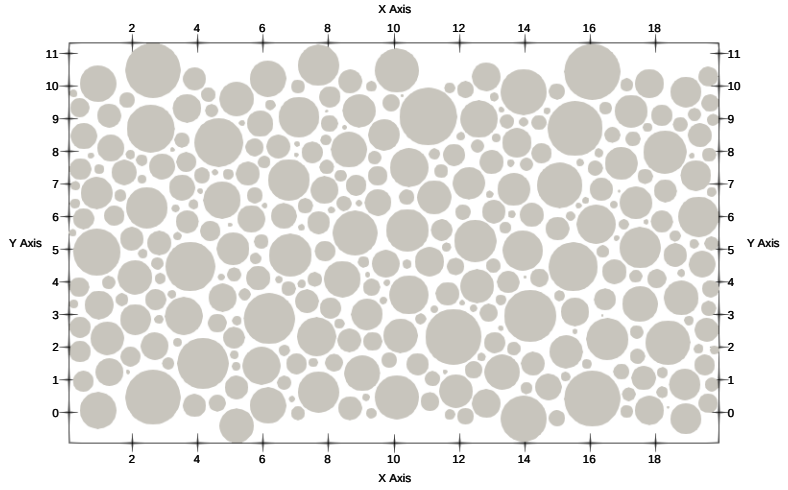


**(b)**

**Figure A.2:** *Two pore-scale domains containing randomly generated circular grains but placed at different positions. The grain size distribution is obtained from a sieve radius analysis of the grains with the same $\theta$. $\theta$ of these images is 0.334, length of the axis are in mm. (b) has the highest permeability ($3.036e^{-11}m^2$), while (a) has the lowest permeability ($2.379e^{-11}m^2$) of this particular MC run.*

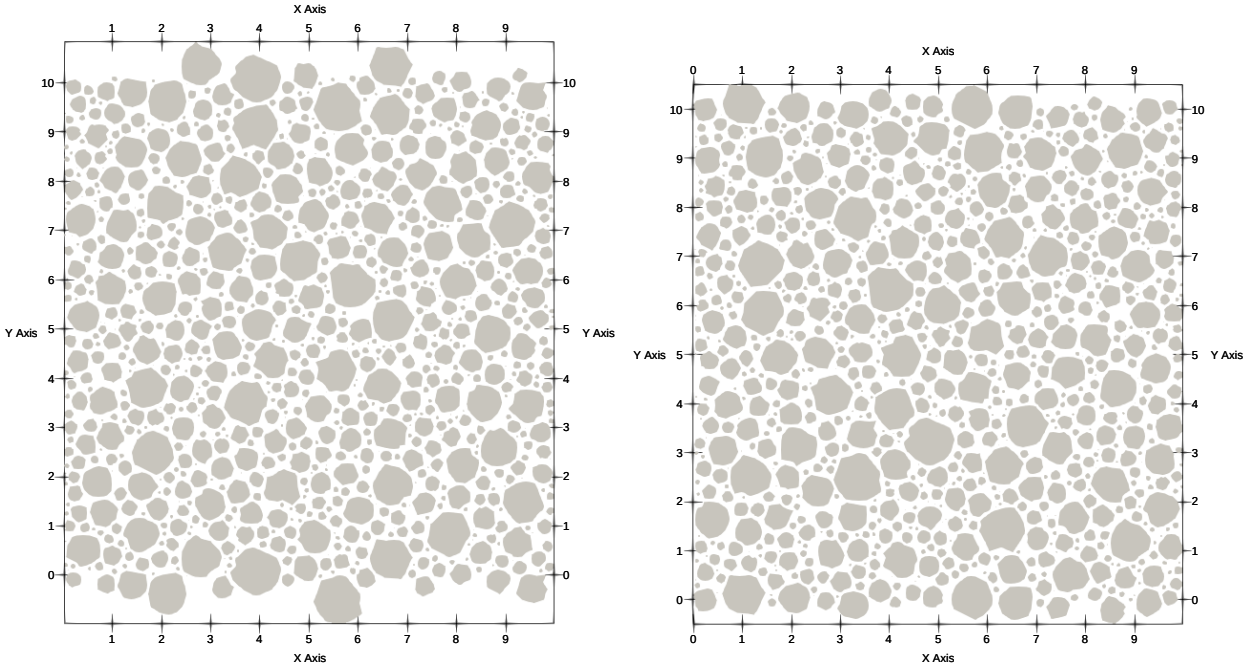


**(a)** **(b)**

**Figure A.3:** *Two pore-scale domains containing randomly generated irregularly shaped grains but placed at different positions. The grain size distribution is generated using a truncated log-normal grain size distribution with values: 0.01, 0.6, 0.45, 0.005 for $r_{min}$, $r_{max}$, $r_{mean}$, and $r_{std}$, respectively. Settings for irregular grain parameters are set to: 0.5, 0.08, 15 for angular spacing, radius variance, and number of shape points, respectively. $\theta$ of these images is 0.424, with (a) has the lowest permeability value ($1.595^{-11}m^2$) of this Monte Carlo simulation, while (b) has the highest permeability value ($1.794e^{-11}m^2$). Cyclicity of the grains can be seen. Domain length and height are given in mm*

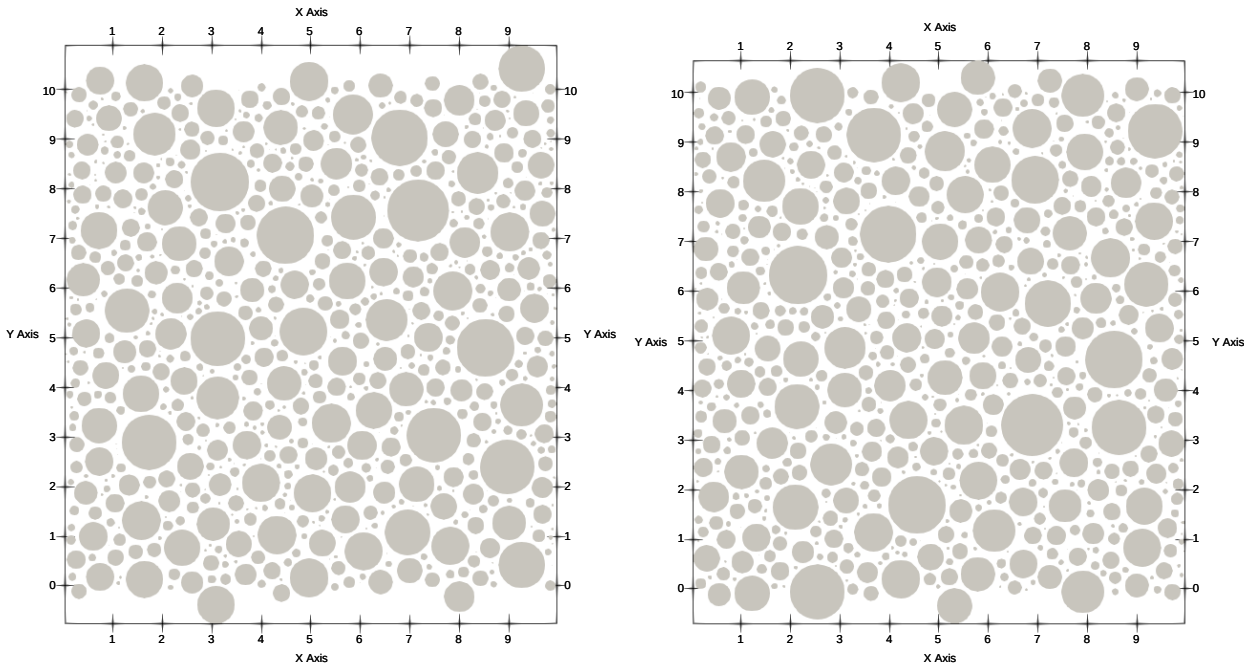


**Figure A.4:** *Two pore-scale domains containing randomly generated circular grains but placed at different positions. The grain size distribution is obtained from a sieve radius analysis of the grains with the same $\theta$. $\theta$ of these images is 0.424, length of the axis are in mm. (a) has the highest permeability ($2.655e^{-11}m^2$), while (b) has the lowest permeability ($3.052e^{-11}m^2$) of this particular MC run.*

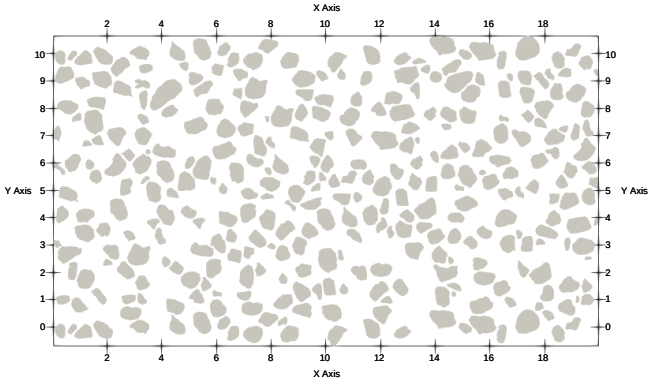


**(a)**

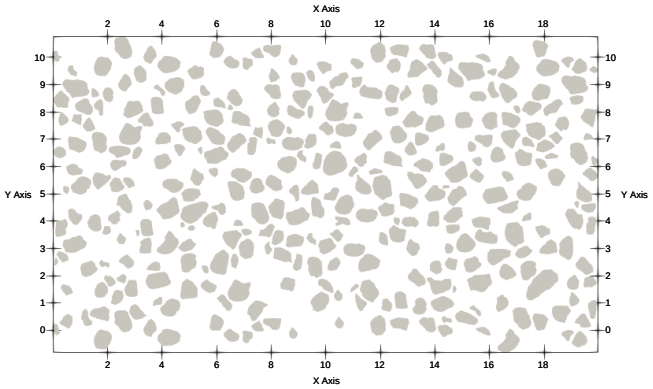


**(b)**

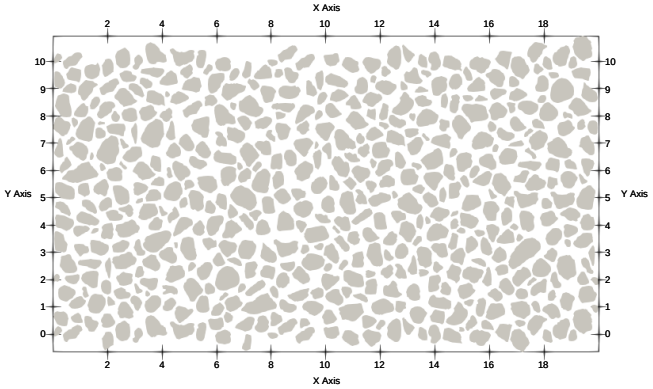


**(c)**

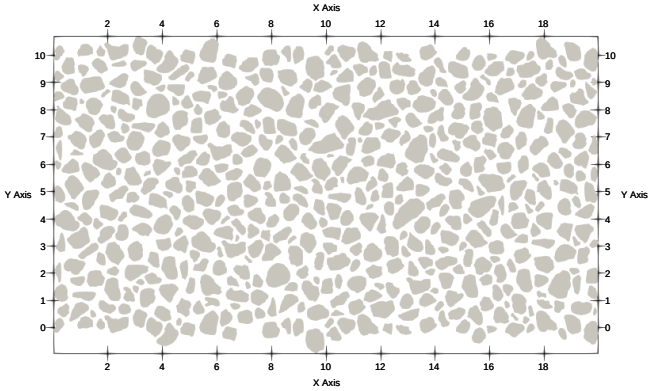


**(d)**

**Figure A.5:** *Pre-generated grained domains. Two realizations with identical grains and porosity, but spatially varied can be observed. Porosity and permeability values are: $\theta = 0.651$ (a),(b) and $k = 2.165e\text{-}10$ (a), $3.273e\text{-}10$ (b) $\theta = 0.466$ (c), (d) and $k = 3.613e\text{-}11$ (c), $4.429e\text{-}11$ (d)*

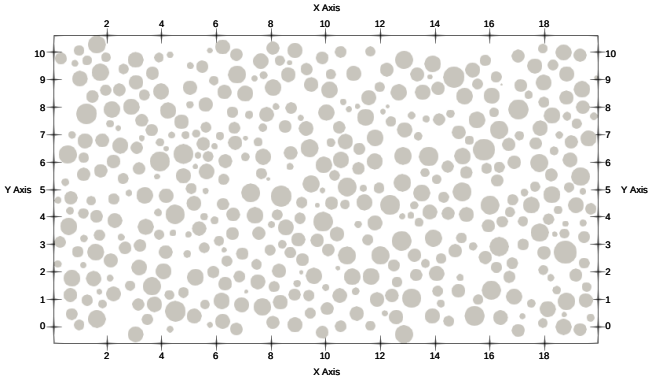


**(a)**

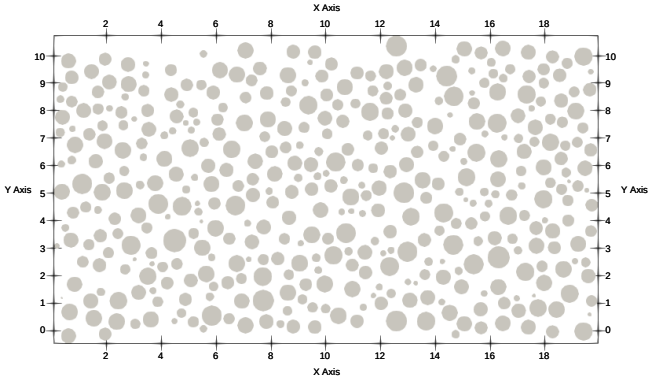


**(b)**

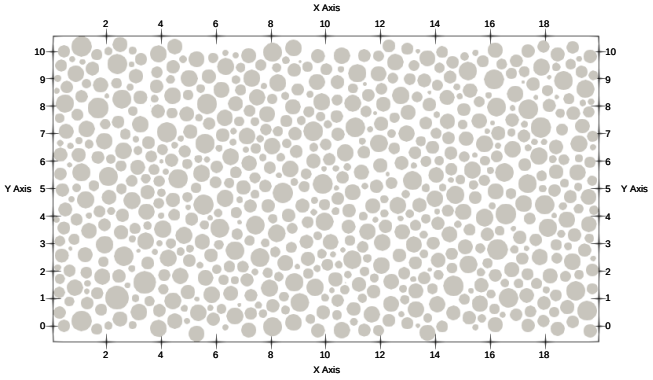


**(c)**

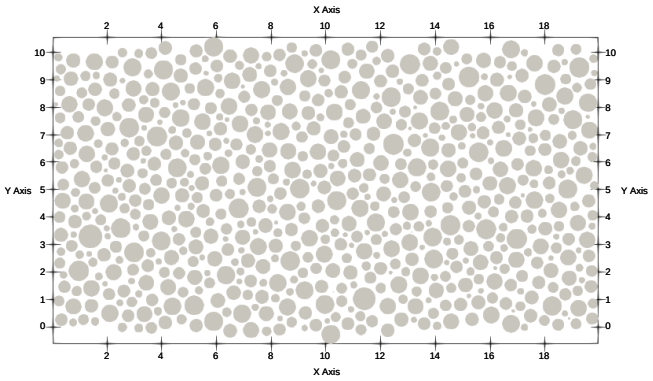


**(d)**

**Figure A.6:** *Pre-generated grained domains. Two realizations with identical grains and porosity, but spatially varied can be observed. Porosity and permeability values are: $\theta = 0.650$ (a),(b) and $k = 2.644e\text{-}10$ (a), $3.380e\text{-}10$ (b) $\theta = 0.465$ (c), (d) and $k = 4.304e\text{-}11$ (c), $5.005e\text{-}11$ (d)*

# References


Ballio, F., and A. Guadagnini, Convergence assessment of numerical Monte Carlo simulations in groundwater hydrology, *Water Resources Research*, *40*(4), doi:10.1029/2003WR002876, 2004.

Barr, D. W., Coefficient of permeability determined by measurable parameters, *Groundwater*, *39*(3), 356–361, 2001.

Bear, J., *Dynamics of Fluids in Porous Media*, Courier Corporation, 1972.

Bear, J., *Modeling Phenomena of Flow and Transport in Porous Media*, Springer, 2018.

Beard, D. C., and P. K. Weyl, Influence of Texture on Porosity and Permeability of Unconsolidated Sand, *AAPG Bulletin*, *57*(2), 349–369, publisher: American Association of Petroleum Geologists, 1973.

Beyer, W., Zur bestimmung der wasserdurchlässigkeit von kiesen und sanden aus der kornverteilungskurve, *WWT*, *14*(6), 165–168, 1964.

Blott, S. J., and K. Pye, Particle shape: a review and new methods of characterization and classification, *Sedimentology*, *55*(1), 31–63, doi:10.1111/j.1365-3091.2007.00892.x, 2008.

Borges, J. A. R., L. F. Pires, F. A. M. Cássaro, W. L. Roque, R. J. Heck, J. A. Rosa, and F. G. Wolf, X-ray microtomography analysis of representative elementary volume (REV) of soil morphological and geometrical properties, *Soil and Tillage Research*, *182*, 112–122, doi:10.1016/j.still.2018.05.004, 2018.

Brown, G. O., H. T. Hsieh, and D. A. Lucero, Evaluation of laboratory dolomite core sample size using representative elementary volume concepts, *Water Resources Research*, *36*(5), 1199–1207, doi:10.1029/2000WR900017, 2000.

Cabalar, A. F., and N. Akbulut, Evaluation of actual and estimated hydraulic conductivity of sands with different gradation and shape, *SpringerPlus*, *5*(1), 820, doi:10.1186/s40064-016-2472-2, 2016.

Chapuis, R. P., and M. Aubertin, On the use of the KozenyCarman equation to predict the hydraulic conductivity of soils, *Canadian Geotechnical Journal*, doi:10.1139/t03-013, publisher: NRC Research Press Ottawa, Canada, 2011.

Chen, H., M. Yang, K. Chen, and C. Zhang, Relative Permeability of Porous Media with Nonuniform Pores, *Geofluids*, *2020*, e5705,424, doi:10.1155/2020/5705424, publisher: Hindawi, 2020.

Chiang, M. Y. M., F. A. Landis, X. Wang, J. R. Smith, M. T. Cicerone, J. Dunkers, and Y. Luo, Local thickness and anisotropy approaches to characterize pore size distribution of three-dimensional porous networks, *Tissue Engineering. Part C, Methods*, *15*(1), 65–76, doi:10.1089/ten.tec.2008.0298, 2009.

Chierici, G. L., *Principles of Petroleum Reservoir Engineering: Volume 1*, Springer Science & Business Media, 2013.

Chilingar, G. V., Relationship Between Porosity, Permeability, and Grain-Size Distribution of Sands and Sandstones, in *Developments in Sedimentology*, *Deltaic and Shallow Marine Deposits*, vol. 1, edited by L. M. J. U. van Straaten, pp. 71–75, Elsevier, doi:10.1016/S0070-4571(08)70469-2, 1964.

Costa, A., Permeability-porosity relationship: A reexamination of the Kozeny-Carman equation based on a fractal pore-space geometry assumption, *Geophysical Research Letters*, *33*(2), doi:10.1029/2005GL025134, 2006.

Costanza-Robinson, M. S., B. D. Estabrook, and D. F. Fouhey, Representative elementary volume estimation for porosity, moisture saturation, and air-water interfacial areas in unsaturated porous media: Data quality implications, *Water Resources Research*, *47*(7), doi:10.1029/2010WR009655, 2011.

Dagan, G., A. Fiori, and I. Janković, Transport in Porous Media, in *Encyclopedia of Ecology*, edited by S. E. Jørgensen and B. D. Fath, pp. 3576–3582, Academic Press, Oxford, doi:10.1016/B978-008045405-4.00300-1, 2008.

Dellino, P., and L. La Volpe, Image processing analysis in reconstructing fragmentation and transportation mechanisms of pyroclastic deposits. The case of Monte Pilato-Rocche Rosse eruptions, Lipari (Aeolian islands, Italy), *Journal of Volcanology and Geothermal Research*, *71*(1), 13–29, doi:10.1016/0377-0273(95)00062-3, 1996.

Devlin, J. F., HydrogeoSieveXL: an Excel-based tool to estimate hydraulic conductivity from grain-size analysis, *Hydrogeology Journal*, *23*(4), 837–844, doi:10.1007/s10040-015-1255-0, 2015.

Dybbs, A., and R. V. Edwards, A New Look at Porous Media Fluid Mechanics — Darcy to Turbulent, in *Fundamentals of Transport Phenomena in Porous Media*, edited by J. Bear and M. Y. Corapcioglu, NATO ASI Series, pp. 199–256, Springer Netherlands, Dordrecht, doi:10.1007/978-94-009-6175-3_4, 1984.

Garcia-Castellanos, D., and U. Lombardo, Poles of inaccessibility: A calculation algorithm for the remotest places on earth, *Scottish Geographical Journal*, *123*(3), 227–233, doi:10.1080/14702540801897809, publisher: Routledge, 2007.

Gilboy, G., The compressibility of sand-mica mixtures, in *Proceedings of the American Society of Civil Engineers*, vol. 54, pp. 555–568, ASCE, 1928.

Gillies, S., et al., Shapely: manipulation and analysis of geometric objects, python Package, 2007.

Gostick, J. T., Z. A. Khan, T. G. Tranter, M. D. r. Kok, M. Agnaou, M. Sadeghi, and R. Jervis, PoreSpy: A Python Toolkit for Quantitative Analysis of Porous Media Images, *Journal of Open Source Software*, *4*(37), 1296, doi:10.21105/joss.01296, 2019.

Graczyk, K. M., and M. Matyka, Predicting porosity, permeability, and tortuosity of porous media from images by deep learning, *Scientific Reports*, *10*, 21,488, doi:10.1038/s41598-020-78415-x, 2020.

Göktepe, A. B., and A. Sezer, Effect of particle shape on density and permeability of sands, *Proceedings of the Institution of Civil Engineers - Geotechnical Engineering*, *163*(6), 307–320, doi:10.1680/geng.2010.163.6.307, publisher: ICE Publishing, 2010.

Hayakawa, Y., and T. Oguchi, Evaluation of gravel sphericity and roundness based on surface-area measurement with a laser scanner, *Computers & Geosciences*, *31*(6), 735–741, doi:10.1016/j.cageo.2005.01.004, 2005.

Hazen, A., XXIII. SOME PHYSICAL PROPERTIES OF SANDS AND GRAVELS, WITH SPECIAL REFERENCE TO THEIR USE IN FILTRATION, in *Volume II State Sanitation: A Review of the Work of the Massachusetts State Board of Health, Volume II*, pp. 232–248, Harvard University Press, doi:10.4159/harvard.9780674600485.c25, 1892.

Heilbronner, R., and S. Barrett, *Image Analysis in Earth Sciences: Microstructures and Textures of Earth Materials*, Springer Science & Business Media, 2013.

Hommel, J., E. Coltman, and H. Class, Porosity–Permeability Relations for Evolving Pore Space: A Review with a Focus on (Bio-)geochemically Altered Porous Media, *Transport in Porous Media*, *124*(2), 589–629, doi:10.1007/s11242-018-1086-2, 2018.

Koponen, A., M. Kataja, and J. Timonen, Permeability and effective porosity of porous media, *Physical Review E*, *56*(3), 3319–3325, doi:10.1103/PhysRevE.56.3319, 1997.

Kozeny, J., Das wasser im boden. grundwasserbewegung, in *Hydraulik*, pp. 380–445, Springer, 1953.

Krauss, E. D., and D. C. Mays, Modification of the Kozeny-Carman Equation To Quantify Formation Damage by Fines in Clean, Unconsolidated Porous Media, *SPE Reservoir Evaluation & Engineering*, *17*(04), 466–472, doi:10.2118/165148-PA, 2014.

Lala, A. M. S., Modifications to the Kozeny–Carman model to enhance petrophysical relationships, *Exploration Geophysics*, *49*(4), 553–558, doi:10.1071/EG17015, publisher: Taylor & Francis, 2018.

Lin, K., Comparative analysis of methods to determine permeability, Master's thesis, Utrecht University, 2021.

Liu, Y. F., and D.-S. Jeng, Pore scale study of the influence of particle geometry on soil permeability, *Advances in Water Resources*, *129*, 232–249, doi:10.1016/j.advwatres.2019.05.024, 2019.

Lopez-Sanchez, M., and S. Llana-Fúnez, Grainsizetools: a python script for estimating the dynamically recrystallized grain size from grain sectional areas, *Solid Earth Discussions*, *6*(2), 3141–3196, doi:10.5194/sed-6-3141-2014, 2014.

Lu, Z., and D. Zhang, On importance sampling Monte Carlo approach to uncertainty analysis for flow and transport in porous media, *Advances in Water Resources*, *11*(26), 1177–1188, doi:10.1016/S0309-1708(03)00106-4, 2003.

Marshall, T. J., Permeability and the Size Distribution of Pores, *Nature*, *180*(4587), 664–665, doi:10.1038/180664a0, number: 4587 Publisher: Nature Publishing Group, 1957.

Matyka, M., A. Khalili, and Z. Koza, Tortuosity-porosity relation in porous media flow, *Physical Review. E, Statistical, Nonlinear, and Soft Matter Physics*, *78*(2 Pt 2), 026,306, doi:10.1103/PhysRevE.78.026306, 2008.

Mgangira, M. B., J. Anochie-Boateng, and J. J. Komba, Quantification of aggregate grain shape characteristics using 3-D laser scanning technology, publisher: SATC 2013, 2013.

Muhammad, N., Finite volume method for simulation of flowing fluid via OpenFOAM, *The European Physical Journal Plus*, *136*(10), 1010, doi:10.1140/epjp/s13360-021-01983-y, 2021.

Nimmo, J., Porosity and Pore Size Distribution, in *Reference Module in Earth Systems and Environmental Sciences*, pp. 295–303, Elsevier, doi:10.1016/B978-0-12-409548-9.05265-9, 2013.

Nishiyama, N., and T. Yokoyama, Permeability of porous media: Role of the critical pore size, *Journal of Geophysical Research: Solid Earth*, *122*(9), 6955–6971, doi:10.1002/2016JB013793, 2017.

Nomura, S., Y. Yamamoto, and H. Sakaguchi, Modified expression of Kozeny–Carman equation based on semilog–sigmoid function, *Soils and Foundations*, *58*(6), 1350–1357, doi:10.1016/j.sandf.2018.07.011, 2018.

Olson, E., PARTICLE SHAPE FACTORS AND THEIR USE IN IMAGE ANALYSIS – PART 1: THEORY, *GXP*, *15*(3), 17, 2011.

pandas development team, T., pandas-dev/pandas: Pandas, doi:10.5281/zenodo.3509134, 2020.

Riley, N. A., Projection sphericity, *Journal of Sedimentary Research*, *11*(2), 94–95, doi:10.1306/D426910C-2B26-11D7-8648000102C1865D, 1941.

Rosas, J., O. Lopez, T. M. Missimer, K. M. Coulibaly, A. H. Dehwah, K. Sesler, L. R. Lujan, and D. Mantilla, Determination of Hydraulic Conductivity from Grain-Size Distribution for Different Depositional Environments, *Groundwater*, *52*(3), 399–413, doi:10.1111/gwat.12078, 2014.

Roussillon, T., H. Piégay, I. Sivignon, L. Tougne, and F. Lavigne, Automatic computation of pebble roundness using digital imagery and discrete geometry, *Computers & Geosciences*, *35*(10), 1992–2000, doi:10.1016/j.cageo.2009.01.013, 2009.

Ruan, K., and X.-L. Fu, A modified Kozeny–Carman equation for predicting saturated hydraulic conductivity of compacted bentonite in confined condition, *Journal of Rock Mechanics and Geotechnical Engineering*, doi:10.1016/j.jrmge.2021.08.010, 2021.

Safari, M., R. Gholami, M. Jami, M. A. Ananthan, A. Rahimi, and W. S. Khur, Developing a porosity-permeability relationship for ellipsoidal grains: A correction shape factor for Kozeny-Carman's equation, *Journal of Petroleum Science and Engineering*, *205*, 108,896, doi:10.1016/j.petrol.2021.108896, 2021.

Shepherd, R. G., Correlations of Permeability and Grain Size, *Groundwater*, *27*(5), 633–638, doi:10.1111/j.1745-6584.1989.tb00476.x, 1989.

Sibiryakov, B., L. W. B. Leite, and E. Sibiriakov, Porosity, specific surface area and permeability in porous media, *Journal of Applied Geophysics*, *186*, 104,261, doi:10.1016/j.jappgeo.2021.104261, 2021.

Slichter, C. S., Geological Survey (U.S.), and Ground Water Branch, *Theoretical investigation of the motion of ground waters*, Washington, D.C, oCLC: 21271918, 1898.

Terzaghi, K., *Erdbaumechanik auf bodenphysikalischer Grundlage*, F. Deuticke, 1925.

Tunwal, M., K. F. Mulchrone, and P. A. Meere, Quantitative characterization of grain shape: Implications for textural maturity analysis and discrimination between depositional environments, *Sedimentology*, *65*(5), 1761–1776, doi:10.1111/sed.12445, 2018.

Urumović, K., and K. Urumović, Comment on "HydrogeoSieveXL: an Excel-based tool to estimate hydraulic conductivity from grain-size analysis": technical note published in Hydrogeology Journal (2015) 23: 837–844, by J. F. Devlin, *Hydrogeology Journal*, *25*(2), 589–591, doi:10.1007/s10040-016-1509-5, 2017.

Urumović, K., and K. Urumović, Comment on 'Reply to Comment on "HydrogeoSieveXL: an Excel-based tool to estimate hydraulic conductivity from grain-size analysis": technical note published in Hydrogeology Journal (2015) 23: 837–844, by J. F. Devlin': article published in Hydrogeology Journal (2017) 25: 593–596, by J. F. Devlin, *Hydrogeology Journal*, *26*(1), 357–358, doi:10.1007/s10040-017-1704-z, 2018.

Virtanen, P., et al., SciPy 1.0: Fundamental Algorithms for Scientific Computing in Python, *Nature Methods*, *17*, 261–272, doi:10.1038/s41592-019-0686-2, 2020.

Wadell, H., Volume, Shape, and Roundness of Rock Particles, *The Journal of Geology*, *40*(5), 443–451, doi:10.1086/623964, publisher: The University of Chicago Press, 1932.

Wang, Q., and L. Tong, Determination Permeability Coefficient from Piezocone, *Advances in Materials Science and Engineering*, *2014*, e396,428, doi:10.1155/2014/396428, publisher: Hindawi, 2014.

Welzl, E., Smallest enclosing disks (balls and ellipsoids), in *New Results and New Trends in Computer Science*, edited by H. Maurer, Lecture Notes in Computer Science, pp. 359–370, Springer, Berlin, Heidelberg, doi:10.1007/BFb0038202, 1991.

Zhang, D., R. Zhang, S. Chen, and W. E. Soll, Pore scale study of flow in porous media: Scale dependency, REV, and statistical REV, *Geophysical Research Letters*, *27*(8), 1195–1198, doi:10.1029/1999GL011101, 2000.

Živković, P., M. Burečić Šafran, and B. Kovačević Zelić, COMPARISON OF MEASURED AND ESTIMATED PERMEABILITY FOR ARTIFICIALLY PREPARED COARSE-GRAINED SOIL SAMPLES, *Rudarsko-geološko-naftni zbornik*, *36*(3), 167–178, doi:10.17794/rgn.2021.3.12, 2021.